
Temporal variability of the carbonate system and air-sea CO₂ exchanges in a Mediterranean human-impacted coastal site

Wimart-Rousseau Cathy ^{1,*}, Lajaunie-Salla Katixa ¹, Marrec Pierre ⁶, Wagener Thibaut ^{1,*}, Raimbault Patrick ¹, Lagadec Véronique ¹, Lafont Michel ¹, Garcia Nicole ¹, Diaz Frédéric ¹, Pinazo Christel ¹, Yohia Christophe ⁴, Garcia Fabrice ¹, Xueref-Remy Irène ², Blanc Pierre-Eric ³, Armengaud Alexandre ⁵, Lefèvre Dominique ^{1,*}

¹ Aix Marseille Univ, Université de Toulon, CNRS, IRD, MIO, UM 110, 13288, Marseille, France

² Aix Marseille Univ, Avignon Université, CNRS, IRD, Institut Méditerranéen de Biodiversité et d'Ecologie Marine et Continentale (IMBE), Marseille, France

³ Observatoire de Haute Provence, OSU Pythéas, France

⁴ Aix Marseille Univ., Université de Toulon, CNRS, IRD, OSU Institut Pythéas, 13288, Marseille, France

⁵ AtmoSud: Observatoire de la Qualité de l'air en Région Sud Provence Alpes Côte d'Azur, le Noilly Paradis, 146 Rue Paradis, 13294, Marseille, Cedex 06, France

⁶ University of Rhode Island, Graduate School of Oceanography, Menden-Deuer Lab, Narragansett, RI, 02882, USA

* Corresponding author : Cathy Wimart-Rousseau : cathy.wimart-rousseau@mio.osupytheas.fr ; Thibaut Wagener : thibaut.wagener@mio.osupytheas.fr ; Dominique Lefèvre : dominique.lefevre@mio.osupytheas.fr

Abstract :

The temporal evolution of the carbonate system and air-sea CO₂ fluxes are investigated for the first time in the Bay of Marseille (BoM – North Western Mediterranean Sea), a coastal system affected by anthropogenic forcing from the Marseille metropolis. This study presents a two-year time-series (between 2016 and 2018) of fortnightly measurements of AT, CT, pH and derived seawater carbonate parameters at the SOLEMIO station. On this land-ocean boundary area, no linear relationship between AT and salinity in surface water is observed due to sporadic intrusions of freshwater coming from the Rhone River. On an annual scale, the BoM acts as a sink of atmospheric CO₂. This result is consistent with previous studies in the Mediterranean Sea. Mean daily air-sea CO₂ fluxes range between -0.8 mmol C.m⁻².d⁻¹ and -2.2 mmol C.m⁻².d⁻¹ during the study period, depending on the atmospheric CO₂ sampling site used for the estimates. This study shows that the pCO₂ in the surface water is predominantly driven by temperature changes, even if partially counterbalanced by biological activity. Therefore, temperature is the main contributor to the air-sea CO₂ exchange variability. Mean daily Net Ecosystem Production (NEP) estimates from CT budget shows an ecosystem in which autotrophic processes are associated with a sink of CO₂. Despite some negative NEP values, the observed air-sea CO₂ fluxes in the BoM are negative, suggesting that thermodynamic processes are the predominant drivers for these fluxes.

Highlights

► First study of the variability of the carbonate system in the Bay of Marseille. ► The Bay of Marseille acts as a sink of atmospheric CO₂ at the annual scale. ► Temperature is the main contributor to the air-sea CO₂ exchange variability.

Keywords : Coastal biogeochemistry, CO₂ fluxes, Carbonate system, North Western Mediterranean Sea, Bay of Marseille

46 1. Introduction

47

48 Since the beginning of the industrial era, human activities have resulted in an increase in
49 carbon dioxide (CO₂) emissions into the atmosphere. The global annual average atmospheric
50 CO₂ concentration of 405 ppm was reached in 2017 (Dlugokencky and Tans, 2019). This
51 increase in CO₂ is likely to be the main factor responsible for current climate change (IPCC,
52 2018). The ocean plays a major role in mitigating climate change via the CO₂ exchanges at
53 the air-sea interface and sequestration into deep water. Between 1994 and 2007, 2.6 ± 0.3
54 PgC.a⁻¹ of CO₂ was absorbed annually (Gruber et al., 2019), representing $31 \pm 4\%$ of the
55 global anthropogenic CO₂ emissions. This absorption of CO₂ by seawater induces an increase
56 in hydronium ion concentration (*i.e.* a decrease in the pH of seawater). As seawater becomes

57 more acidic, it causes carbonate ions to be relatively less abundant, which has a significant
58 impact on biological and physio-chemical processes (Doney et al., 2009). This process is
59 called “ocean acidification”. Carbon budgets in near-shore areas such as seagrass beds (Huang
60 et al., 2015; Kirkman and Reid, 1979) and coral reefs (Suzuki and Kawahata, 2003; Ware et
61 al., 1992) are well documented, but coastal oceanic areas that cover about 7 % of the oceanic
62 domain (Wollast, 1998) are usually neglected when producing global carbon budgets.
63 However, recent studies have highlighted that coastal seas act as a sink of CO₂ with a range of
64 between 0.2 and 0.4 PgC.a⁻¹ (Borges et al., 2006), with a recent regionalised global CO₂ sink
65 estimate of 0.19 ± 0.05 PgC.a⁻¹ (Laruelle et al., 2014), that is between 8 % and 15 % of the
66 oceanic CO₂ sink. Although open-ocean CO₂ inventories and dynamics have been studied in
67 detail over the last 30 years (Gruber et al., 2019; Takahashi et al., 2002), the importance of
68 coastal oceanic areas has been underestimated (Bourgeois et al., 2016; Gattuso et al., 1998).
69 In contrast to open-ocean acidification trends ranging from -0.0004 (Astor et al., 2013) to -
70 0.0026 pH units.a⁻¹ (Olafsson et al., 2010), rates of change in pH of coastal systems range
71 from -0.023 to 0.023 pH units.a⁻¹ (Carstensen and Duarte, 2019). Coastal areas are under the
72 influence of multiple and diverse forcing variables due to their interactions with the land and
73 human activities (Borges et al., 2006; Bourgeois et al., 2016).

74 The Mediterranean Sea (MedSea) more specifically is subjected to significant land-ocean
75 interactions along its coastal areas. Because of its semi-enclosed nature and smaller inertia,
76 due to the relatively short residence time of its water masses, it is highly reactive to external
77 forcing variables in particular variations in water, energy and matter fluxes at the interfaces
78 (Durrieu de Madron et al., 2011). The role of the MedSea as a source or sink for atmospheric
79 CO₂ in the global carbon cycle, especially in the context of warming MedSea waters, is
80 unclear (Nykjaer, 2009; Vargas-Yáñez et al., 2008). Several recent studies indicate a gradual
81 change from a source to a sink over the last few decades (Louanchi et al., 2009; Taillandier et
82 al., 2012). However, *in situ* measurements of the carbonate seawater system are still scarce for
83 the MedSea. In recent years, a few cruises have given a clearer description of the carbonate

84 system at the basin scale (Álvarez et al., 2014). For the North Western (NW) part of the basin,
85 time-series of carbonate chemistry exist in the Ligurian Sea at the DYFAMED and
86 ANTARES sites (Fig.1 – e.g., Copin-Montégut and Bégovic, 2002; Coppola et al., 2018;
87 Hood and Merlivat, 2001; Lefèvre, 2010; Merlivat et al., 2018; Touratier and Goyet, 2009), in
88 the Bay of Villefranche-sur-Mer at the Point B station (Fig.1 - De Carlo et al., 2013;
89 Kapsenberg et al., 2017) and in the Gulf of Trieste at the coastal C1 station (Ingrosso et al.,
90 2016).

91 The Bay of Marseille (BoM) is located in the NW MedSea on the Gulf of Lions continental
92 shelf and is adjacent to the metropolis of Marseille, the second biggest city in France (Fig.1)
93 with a population of over 1 million inhabitants. Due to this proximity, the BoM sporadically
94 receives (especially during flood events) effluents from the sewage system and coastal rivers
95 enriched in nutrients, organic matter and chemical products (Millet et al., 2018). The bay also
96 experiences strong winds (Petrenko, 2003) and large seasonal temperature variations
97 (<http://somlit.oas.u-bordeaux.fr/mysomlit-public/>). Northern Current intrusions (Petrenko,
98 2003) also contribute to a non-negligible influence on the shelf circulation.

99 Finally, in addition to these complex dynamics, under specific conditions, water masses in the
100 BoM can be influenced by the extension to the East of the Rhone River plume (Frayssé et al.,
101 2014; Gatti et al., 2006), even though the Rhone River estuary is 35 km West of the BoM and
102 does not flow directly into the BoM. The Rhone River is the major input of freshwater into
103 the Western MedSea with a mean annual discharge of $1700 \text{ m}^3 \cdot \text{s}^{-1}$ which can reach more than
104 $11\,200 \text{ m}^3 \cdot \text{s}^{-1}$ during centennial flooding (Pont et al., 2002).

105 In consequence, the ecosystem of the BoM is subject to large daily and seasonal variability in
106 the physical and chemical forcing. These will directly affect biological processes such as
107 photosynthesis, respiration or CaCO_3 precipitation and dissolution (Bensoussan and Gattuso,
108 2007). Moreover, due to the nearby highly urbanised area, high atmospheric CO_2
109 concentrations (up to 540 ppm) with large daily variability have been observed and may
110 directly affect seawater $p\text{CO}_2$.

111 The SOLEMIO station located in the BoM (Fig.1) is part of the French national network of
Journal Pre-proof
112 coastal observation SOMLIT (Service d'Observation en Milieu Littoral –
113 <http://somlit.epoc.u-bordeaux1.fr/fr/>). This network was implemented in 1994 for the
114 monitoring of physical, chemical and biological parameters. Within this network, core
115 parameters are collected in order to address the long-term evolution of coastal ecosystems.
116 Measurements of carbonate chemistry parameters are not routinely measured within the
117 framework of the SOMLIT network.

118 This paper presents a two-year time-series of carbonate chemistry data acquired between June
119 2016 and July 2018 in the BoM at SOLEMIO with the aim of deciphering the main physical
120 and biological processes driving this carbonate system time-series. In light of the current
121 knowledge concerning carbonate chemistry in the MedSea, the results will (1) study the
122 seasonality of the carbonate system and highlight the impact events in the bay, (2) evaluate
123 the CO₂ exchanges between this coastal system and the atmosphere and (3) estimate, with
124 numerous assumptions, the importance of biological processes on CO₂ exchanges in the BoM.
125 The limitations highlighted in this study will support the discussion for recommending future
126 studies in this dynamic coastal ecosystem.

127

128 **2. Methods**

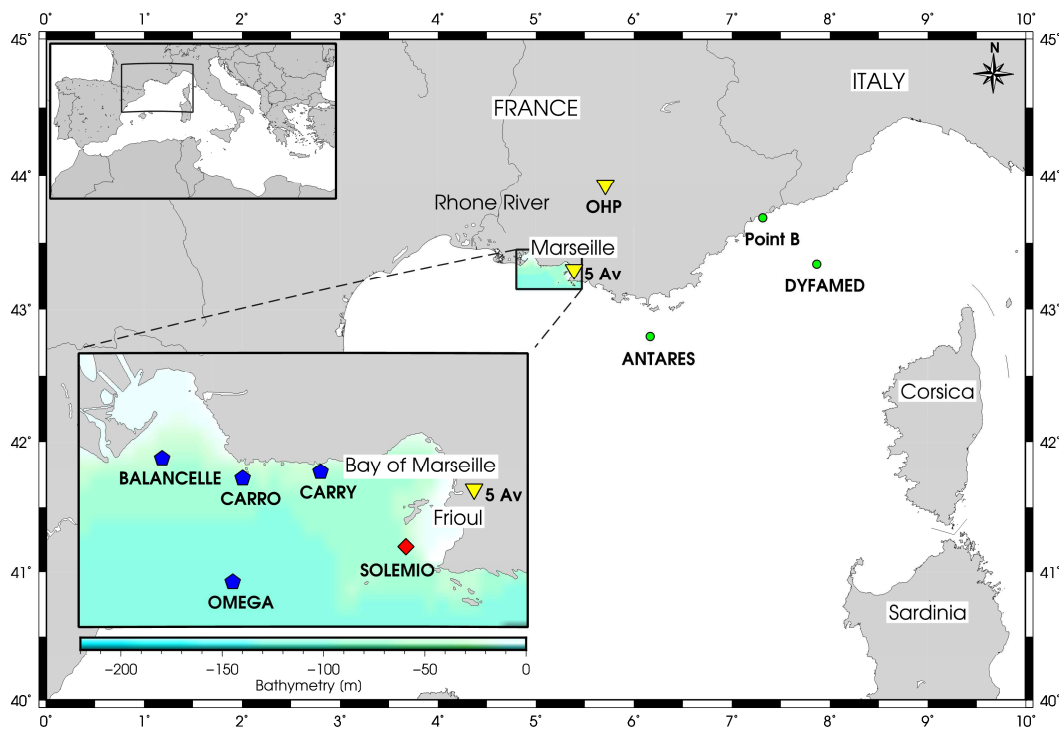
129

130 2.1. Sampling strategy and oceanic data acquisition

131

132 Sampling and measurements were carried out fortnightly at the SOLEMIO station in the NW
133 MedSea (43°14.10'N – 5°17.30'E, 55 m bottom depth; Fig.1) from the R.V. Antedon II from
134 June 6th, 2016 to July 11th, 2018. Physical properties of the water column (temperature,
135 conductivity, depth) were measured *in situ* with a SeaBird 9 or a SeaBird 19+ profiler.
136 Sensors were calibrated at least every 2 years (last calibration in January 2017). Conductivity
137 (SBE4 sensor, Seabird®) and temperature (SBE3 sensor, Seabird®) measurements were

138 recorded with a precision of 0.0003 S.m^{-1} and 0.001°C , respectively. Calibration reports
 139 *Journal Pre-proof*
 140 indicate a mean annual drift for the temperature and conductivity sensors of $\pm 0.001^\circ\text{C}$ and of
 141 $\pm 0.002 \text{ S.m}^{-1}$, respectively. Salinity is expressed using the Practical Salinity Scale. Data is
 142 reported as mean \pm standard deviation.
 143 Discrete water samples were collected at 3 depths (surface layer, intermediate layer and
 144 bottom layer), using 12 dm^3 Niskin® bottles attached to the rosette. Only discrete water
 145 samples collected at 2 depths (1 m and 55 m) were used.



146

Figure 1. The area of the North Western Mediterranean Sea showing the Southern coast of France, Corsica and Sardinia, the location of the DYPAMED ($43^\circ25'N - 7^\circ52'E$), Point B ($43^\circ41.10'N - 7.18.94'E$) and the ANTARES ($42^\circ50'N - 6^\circ10'E$) study sites, the SOLEMIO station ($43^\circ14.30'N - 5^\circ17.30'E$) and the STPS network with its four buoys: the Balancelle buoy ($43^\circ20.443'N - 4^\circ55.464'E$), the Omega buoy ($43^\circ11.952'N - 5^\circ01.789'E$), the Carro buoy ($43^\circ18.716'N - 5^\circ09.641'E$) and the Carry buoy ($43^\circ19.146'N - 5^\circ09.641'E$). The OHP ($43^\circ55.9'N - 5^\circ42.8'E$) and 5 Av ($43^\circ18.4'N - 5^\circ23.7'E$) are the sites that measure atmospheric CO_2 . The bathymetry of the area is in meters.

148

149 Samples for dissolved inorganic carbon (C_T) and total alkalinity (A_T) were collected into acid
150 washed 500 cm³ borosilicate glass bottles and poisoned with 200 mm³ of a 36 g.m⁻³ HgCl₂, as
151 recommended by Dickson et al. (2007). Samples were stored in the dark at 4°C for 1 to 6
152 months before analysis. Measurements of C_T and A_T were performed simultaneously by
153 potentiometric acid titration using a closed cell following the methods described by Edmond
154 (1970) and DOE (1994). Analyses were performed at the National facility for analysis of
155 carbonate system parameters (SNAPO-CO₂, LOCEAN, Sorbonne University – CNRS,
156 France) with a prototype developed at LOCEAN. Average accuracy of A_T and C_T analysis
157 was 2.3 and 2.6 μmol.kg⁻¹, respectively, validated using Certified Reference Material (CRM)
158 provided by A. Dickson's laboratory (Scripps Institution of Oceanography, San Diego).

159 The pH was measured spectrophotometrically at the MIO (Mediterranean Institute of
160 Oceanography, Marseille – France). Unpurified m-cresol purple (McP) dye (Sigma®) at
161 standard temperature (25°C) was used and results are reported on the total hydrogen ion
162 concentration scale (pH_T). Measurements were performed following the protocol described by
163 Clayton and Byrne (1993) based on the dissociation of the pH-sensitive indicator dye in the
164 water sample. Within the pH-range of seawater, the dye dissociates into a protonated and an
165 unprotonated form which have different absorbance spectra in the visible range. The ratio of
166 absorbance between 578 and 434 nm was used to determine seawater pH. The parameter pH_T
167 was calculated following Dickson et al. (2007). The reproducibility of the measurements
168 based on replicates measurements was 0.001 (mean value = 8.047, n = 8).

169 Unfiltered samples were collected for nutrient analysis in 60 cm³ polyethylene flasks and
170 immediately frozen. Nutrient concentrations were obtained following the protocol of Aminot
171 and K  rouel (2007). Detection limits for nitrite (NO₂⁻), nitrate (NO₃⁻), and silicate (Si(OH)₄)
172 were of 0.05 μM and 0.003 - 0.006 μM for phosphate (PO₄³⁻); the relative precision of these
173 analyses ranged from 5 % to 10 % (Aminot and K  rouel, 2007). Analysis of nutrients follows

174 the protocols and the quality assurance process set by the SOMLIT network
Journal Pre-proof
175 (<http://somlit.epoc.u-bordeaux1.fr>).

176 Over these two-years of sampling, 140 samples distributed over the 3 depths of the water
177 column (surface layer, intermediate layer and bottom layer) were obtained.

178

179 2.3. Ancillary data

180

181 Average weekly wind speeds at 10 meters altitude above the water surface (U_{10} , in $\text{m}\cdot\text{s}^{-1}$) and
182 daily precipitation at the SOMLIT site were obtained from the WRF (Weather Research
183 Forecast) model (gridded by 2×2 km). Total atmospheric pressure (P_T , in atm) was obtained
184 from the Meteo France station (WMS07650) at the Marseille-Marignane Airport ($43^\circ 26.4' \text{N} -$
185 $5^\circ 13.8' \text{E}$). Atmospheric CO_2 data (mole fraction of CO_2 in dry air in ppm, $[\text{CO}_2]_{\text{atm}}$) from the
186 OHP site ($43^\circ 55.9' \text{N} - 5^\circ 42.8' \text{E}$; Observatoire de Haute Provence, ST Michel l'Observatoire
187 – France) and 5 Av site ($43^\circ 18.4' \text{N} - 5^\circ 23.7' \text{E}$; Cinq Avenues, Marseille – France; Fig.1)
188 were retrieved from the ICOS National Network, France ([http://www.obs-](http://www.obs-hp.fr/ICOS/Plaquette-ICOS-201407_lite.pdf)
189 [hp.fr/ICOS/Plaquette-ICOS-201407_lite.pdf](http://www.obs-hp.fr/ICOS/Plaquette-ICOS-201407_lite.pdf)) and the AtmoSud Regional Atmospheric Survey
190 Network, France (<https://www.atmosud.org>), respectively. The conversion of $[\text{CO}_2^{\text{atm}}]$ (mole
191 fraction of CO_2 in ppm) into $p\text{CO}_2$ (partial pressure of CO_2) was done according to the
192 equation (1):

193

$$194 \quad p\text{CO}_2^{\text{ATM}} = [P_T - (H/100) \times P_{\text{H}_2\text{O}}] \times [\text{CO}_2^{\text{atm}}] \quad (1)$$

195

196 where $p\text{CO}_2^{\text{ATM}}$ is the atmospheric partial pressure of CO_2 (in μatm), P_T is the total
197 atmospheric pressure in atm), H is the relative humidity (here 100 %) and $P_{\text{H}_2\text{O}}$ is the vapour
198 pressure of water at ambient temperature (in atm). $P_{\text{H}_2\text{O}}$ was determined from surface seawater
199 temperature (Dean and Lange, 1999). The estimated total error of the atmospheric $p\text{CO}_2$
200 calculated is $2 \mu\text{atm}$.

201 A network composed of 4 STPS probes (Salinity, Temperature and Pressure Sensors, NKE®)
202 was installed onto sub-surface buoys (the Balancelle, Carro, Carry and Omega buoys) along
203 the coast between the mouth of the Rhone River and the BoM. This network follows and
204 identifies discharges from the Rhone River by measuring hourly temperature and salinity data.
205 The SOLEMIO site (Fig.1) completes this network inside the BoM.

206

207 2.4. Derived data

208

209 2.4.1. Mixed layer depth

210

211 In this study, the mixed layer depth (MLD) is defined as the depth where the temperature is
212 0.5°C lower than the sea surface (1 m) temperature (Monterey and Levitus, 1997). Vertical
213 profiles of temperature in the water column from the CTD were used to estimate the MLD.

214

215 2.4.2. Carbonate system parameters

216

217 Derived seawater carbonate system parameters (seawater partial pressure of CO₂ ($p\text{CO}_2^{\text{SW}}$)
218 and saturation states for calcite and aragonite) were estimated from A_T and C_T values.
219 Calculations were made with the software program CO2SYS (version 2.1) (Pierrot et al.,
220 2006), considering silicate and phosphate concentrations. As recommended by Álvarez et al.
221 (2014) for the MedSea, the carbonic acid dissociation constants K_1 and K_2 from Mehrbach et
222 al. (1973) as refitted by Dickson and Millero (1987) and the dissociation constant for HSO_4^-
223 form Dickson (1990) were used.

224

225 Although the pH- C_T couple gives more accurate estimations for seawater $p\text{CO}_2$ (Millero,
226 1995), A_T and C_T values were used. This choice was justified as measured pH values can be
227 subject to inaccuracy (see Fig.1 supplementary material) due to the use of unpurified McP

228 (Yao et al., 2007) whereas the accuracy of A_T and C_T measurements is controlled through the
229 use of CRM. Thus, the estimated total error of the calculated pCO_2^{SW} is 5.8 μatm (Millero,
230 1995). All the derived carbonate parameters are presented at *in situ* temperature.

231

232 2.4.3. Deconvolution of thermal and non-thermal processes on pCO_2^{SW}

233

234 Effects of non-thermal (pCO_2^N) and thermal (pCO_2^{TD}) processes on pCO_2^{SW} variations have
235 been calculated thereafter using following equations (2) and (3) (Takahashi et al., 1993,
236 2002):

237

$$238 \quad pCO_2^N = pCO_2^{obs} \times e^{(0.0423(T_{mean} - T_{obs}))} \quad (2)$$

239

$$240 \quad pCO_2^{TD} = pCO_2^{mean} \times e^{(0.0423(T_{obs} - T_{mean}))} \quad (3)$$

241

242 where pCO_2^{obs} is the pCO_2^{SW} calculated during the study period in surface (in μatm),
243 pCO_2^{mean} is the mean pCO_2^{SW} over the study period in surface (402 μatm), T^{mean} is the average
244 temperature (in $^\circ\text{C}$, here $T^{mean} = 16.90^\circ\text{C}$) and T^{obs} is the *in situ* temperature (in $^\circ\text{C}$).

245 pCO_2^N represents a temperature-normalised pCO_2^{SW} , and pCO_2^{TD} represents the changes
246 pCO_2^{SW} induced by temperature fluctuations under isochemical conditions.

247

248 2.4.4. CO_2 fluxes between ocean and atmosphere

249

250 The air-sea CO_2 exchanges were calculated according to the equation described in Weiss
251 (1974) and Wanninkhof (2014). The flux of CO_2 , expressed in this paper in $\text{mmol } CO_2 \cdot \text{m}^{-2} \cdot \text{d}^{-1}$,
252 can be determined according to the equation (4):

253

$$254 \quad FCO_2 = k \times \alpha \times (pCO_2^{SW} - pCO_2^{ATM}) \quad (4)$$

256 where k is the gas transfer velocity for CO_2 (in cm.h^{-1}), α is the solubility coefficient of CO_2
 257 (in $\text{mol.L}^{-1}.\text{atm}^{-1}$) calculated as a function of temperature and salinity (Weiss, 1974) and
 258 $p\text{CO}_2^{\text{SW}}$ and $p\text{CO}_2^{\text{ATM}}$ are the seawater and atmospheric partial pressure of CO_2 , respectively
 259 (in μatm). By convention, a negative sign indicates a flux from the atmosphere to the ocean
 260 (Wanninkhof et al., 2013).

261

262 The relationship (5) of Wanninkhof (2014) is used to compute the gas transfer velocities:

263

$$264 \quad k = 0.251 \times U_{10}^2 \times (\text{Sc}/660)^{-1/2} \quad (5)$$

265

266 where U_{10} is the wind speed (in m.s^{-1}) and Sc is the Schmidt number (dimensionless),
 267 calculated according to the equation in Wanninkhof (2014).

268 The air-sea CO_2 fluxes were estimated at the same time as the $p\text{CO}_2^{\text{SW}}$ estimation. Because
 269 no atmospheric $p\text{CO}_2$ measurement is available at the SOLEMIO point, the mean $p\text{CO}_2^{\text{ATM}}$
 270 value (see section 2.3) for the week preceding the measurement of $p\text{CO}_2^{\text{SW}}$ was used, this val-
 271 ue being an estimate of the regional average $p\text{CO}_2^{\text{ATM}}$ value for the sampling day. Due to the
 272 buffering effect, the weekly average wind speed estimate at the SOLEMIO was used in air-sea
 273 fluxes calculations.

274

275 2.4.5. Biological flux calculations

276

277 Net Ecosystem Calcification (NEC) of the system was calculated according to Eq.6 (derived
 278 from Bensoussan and Gattuso (2007):

279

$$280 \quad \text{NEC} = -0.5 \times \Delta A_T \times d \times \rho / \Delta t \quad (6)$$

281

282 where ΔA_T is the change in total alkalinity between sampling intervals (in mmol.kg^{-1}), d is the
283 mixed layer depth (MLD) water (in meters), ρ is the *in situ* seawater density (in kg.m^{-3}) and
284 Δt is the time interval between sample intervals (in days). NEC is in $\text{mmol C.m}^{-2}.\text{d}^{-1}$.

285

286 Net Ecosystem Production (NEP) was calculated according to Eq.7 (derived from Borges et
287 al., 2008) using changes in C_T from two consecutive samplings and correcting for additional
288 changes associated with NEC and air-sea CO_2 gas exchanges (FCO_2) as:

289

$$290 \text{ NEP} = - [\Delta C_T \times d \times \rho / \Delta t - \text{NEC} + \text{FCO}_2] \quad (7)$$

291

292 where ΔC_T is the change in C_T (in mmol.kg^{-1}) over the time period Δt (in days), d is the mixed
293 layer depth (MLD) water (in meters), ρ is the *in situ* seawater density (in kg.m^{-3}), NEC is in
294 $\text{mmol C.m}^{-2}.\text{d}^{-1}$ and FCO_2 is the average air-sea flux of CO_2 between two consecutive sam-
295 plings (in $\text{mmol CO}_2.\text{m}^{-2}.\text{d}^{-1}$). NEP is in $\text{mmol C.m}^{-2}.\text{d}^{-1}$. To remove the impact of salinity
296 variations (evaporation/precipitation) on A_T , salinity-normalised changes in A_T (and C_T) were
297 calculated by dividing by *in situ* salinity and multiplying by 38. The remaining ΔA_T is as-
298 sumed to be from calcification/dissolution. Nonetheless, because no significant relationship
299 exists between C_T and the sea surface salinity at the SOLEMIO site, C_T has not been normal-
300 ised to salinity for NEP calculations. Low Salinity Events (see section 4.2) have been re-
301 moved from these calculations.

302

303 2.4.6. Statistic test

304

305 Linear relationships have been tested using the Pearson coefficient for parametric test (Sokal
306 and Rohlf, 1969) with a significance level of 95 %.

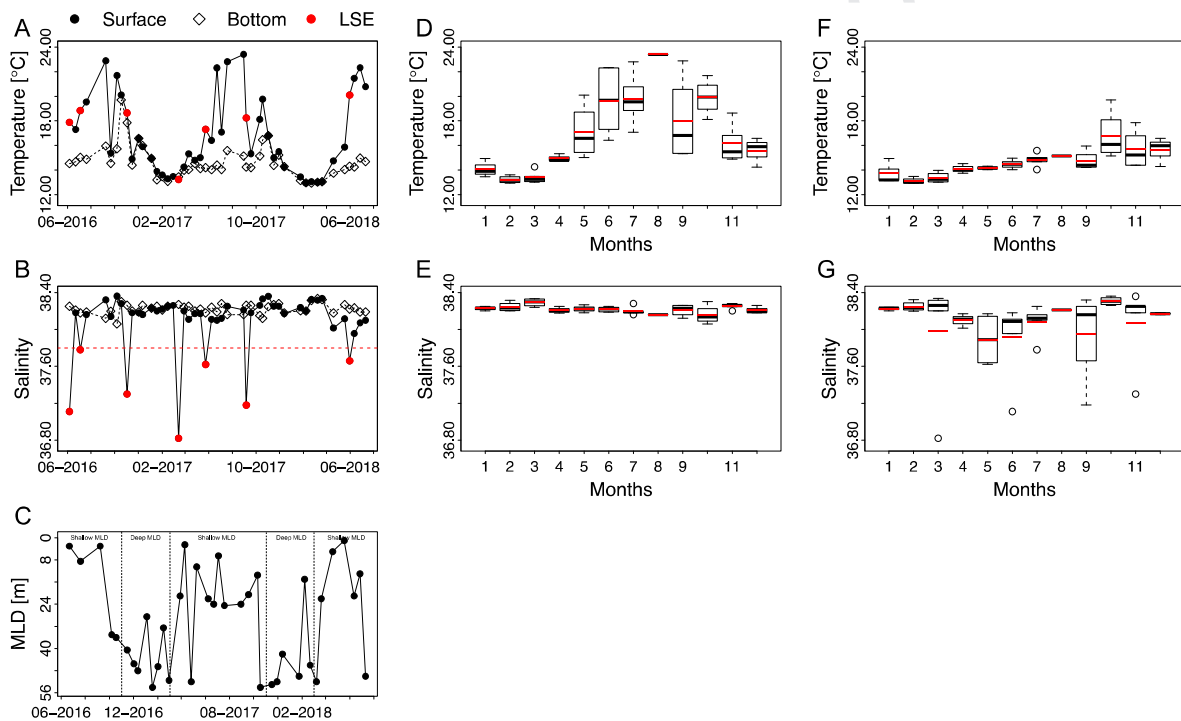
307

308
309
310
311
312
313
314
315
316

3. Results

3.1. Hydrography

The hydrographic conditions encountered at the SOLEMIO site are described in Figure 2 with the time-series of temperature, salinity and MLD over the studied period (Fig.2A, 2B and 2C) and the monthly mean values for temperature and salinity at the surface and bottom (Fig.2D, 2E, 2F and 2G).



317

Figure 2. Time-series observations for temperature (A), salinity (B) and Mixed Layer Depth (MLD - C) and box plots of pooled monthly temperature and salinity at the SOLEMIO site at 1 m (black circles and solid line; Fig.2D & 2E) and at the bottom (55 m – white diamonds and dotted line; Fig.2F & 2G) from June 2016 to July 2018. In figures (A) and (B), red points represent Low Salinity Events (LSE), and the red dotted line represents a salinity equal to 37.8. In box plots are shown the median (black line), the mean (red line), the first (Q1), and third quartiles (Q3) and data outliers (dotted lines).

318 Over the two-years, the mean temperature was 16.90°C at the surface and 14.65°C at the bot-
Journal Pre-proof
319 tom, with a maximum (23.42°C) and minimum (12.94°C) occurring both in surface waters in
320 August 2017 and February 2018, respectively. Marked seasonal cycles were present for both
321 depths (Fig.2A, 2D and 2F) with an increase in temperature from May to October and a de-
322 crease from November to April. Based on the temperature data recorded at the SOLEMIO site
323 from January 1997 to October 2019 (<http://somlit.oasu.u-bordeaux.fr/mysomlit-public/>), the
324 hydrological situation for the period used in this manuscript shows that summers and winters
325 were warmer than the reference situation in 1997, with an increase over the two-years. No
326 extreme climatic event has been reported over the studied period.

327 Based on monthly means (Fig.2E and 2G), the annual range in salinity at the SOLEMIO site
328 was higher at the surface (from 36.82 to 38.36) than at the bottom (from 38.06 to 38.33). Over
329 the two-year period, lower mean values of salinity are observed in the surface (38.07) than at
330 the bottom (38.22) (Table 1). In this study, “Low Salinity Events” (LSE) will represent the
331 sampling day where the recorded values of salinities were lower than 37.80 at the surface.
332 LSE were recorded seven times at the SOLEMIO station over the studied period, mostly in
333 spring and summer (Fig.2B).

334

Table 1. Time-series analyses on seawater carbonate chemistry at the SOLEMIO site for temperature (Temp.), salinity, pH_{Tis} measured in situ (pH_{Tis}), total alkalinity (A_T), dissolved inorganic carbon (C_T), partial pressure of CO_2 (pCO_2), nitrate (NO_3^-), nitrite (NO_2^-), phosphate (PO_4^{3-}), orthosilicic acid ($SiOH_4$), calcite (Ω_C) and aragonite (Ω_A) saturation states, from June 2016 to July 2018, at 1 m and at the bottom (55 m). SD stands for standard deviation. DL stands for Detection Limit.

SURFACE			BOTTOM		
	Mean \pm SD	Min. – Max.		Mean \pm SD	Min. – Max.
Temp. [$^{\circ}C$]	16.90 \pm 3.16	12.94 – 23.42	Temp. [$^{\circ}C$]	14.65 \pm 1.33	12.93 – 19.71
Salinity	38.07 \pm 0.34	36.82 – 38.36	Salinity	38.22 \pm 0.06	38.06 – 38.33
pH_{Tis}	8.086 \pm 0.028	8.015 – 8.121	pH_{Tis}	8.091 \pm 0.018	8.053 – 8.129
A_T [$\mu mol.kg^{-1}$]	2584 \pm 18	2554 – 2624	A_T [$\mu mol.kg^{-1}$]	2582 \pm 15	2560 – 2621
C_T [$\mu mol.kg^{-1}$]	2289 \pm 27	2248 – 2359	C_T [$\mu mol.kg^{-1}$]	2303 \pm 20	2256 – 2358
pCO_2 [μatm]	402 \pm 31	358 – 471	pCO_2 [μatm]	394 \pm 21	362 – 439
NO_3^- [$\mu mol.L^{-1}$]	0.78 \pm 1.07	<DL – 5.48	NO_3^- [$\mu mol.L^{-1}$]	1.16 \pm 0.94	0.03 – 3.5
NO_2^- [$\mu mol.L^{-1}$]	0.09 \pm 0.12	<DL – 0.64	NO_2^- [$\mu mol.L^{-1}$]	0.14 \pm 0.11	0.01 – 0.42
PO_4^{3-} [$\mu mol.L^{-1}$]	0.05 \pm 0.04	<DL – 0.21	PO_4^{3-} [$\mu mol.L^{-1}$]	0.05 \pm 0.04	<DL – 0.14
$SiOH_4$ [$\mu mol.L^{-1}$]	1.63 \pm 0.65	0.41 – 4.50	$SiOH_4$ [$\mu mol.L^{-1}$]	1.86 \pm 0.59	0.43 – 3.46
Ω_C	4.99 \pm 0.33	4.44 – 5.64	Ω_C	4.67 \pm 0.23	4.23 – 5.29
Ω_A	3.23 \pm 0.24	2.85 – 3.70	Ω_A	3.01 \pm 0.16	2.72 – 3.45

335

336 Based on MLD estimates, two hydrological “seasons” can be defined in the BoM: a well-
 337 mixed water column in winter (“winter” deep MLD between November and March included)
 338 and a summer thermal stratification period (“summer” shallow MLD between April and
 339 October included) with average MLD values of 41 ± 13 m in “winter” deep MLD conditions
 340 and of 20 ± 17 m in “summer” shallow MLD (Fig.2C).

341

342 3.2. Nutrients

343

344 The variations in inorganic nutrient concentrations over the studied period are described in the
 345 Figure 2 of the supplementary material with a time-series for NO_3^- , NO_2^- , PO_4^{3-} and $Si(OH)_4$.
 346 NO_3^- , NO_2^- and PO_4^{3-} concentrations displayed smooth seasonal patterns, with a decrease
 347 during spring (March - April) reaching a minimum value, under the detection limit, in late
 348 spring or summer and an increase in autumn reaching a maximum value in winter (January –
 349 February). At the surface, concentrations ranged from non-detectable to $5.48 \mu mol.L^{-1}$ for
 350 nitrate, from non-detectable to $0.64 \mu mol.L^{-1}$ for nitrite and from non-detectable to 0.21
 351 $\mu mol.L^{-1}$ for phosphate. Orthosilicic acid concentrations were never completely depleted in

352 the water column. NO_3^- , NO_2^- and PO_4^{3-} concentrations were low at both depths throughout
 353 the studied period with lower concentrations at the surface than at the bottom (Table 1).

354

355 3.3. Carbonate system parameters

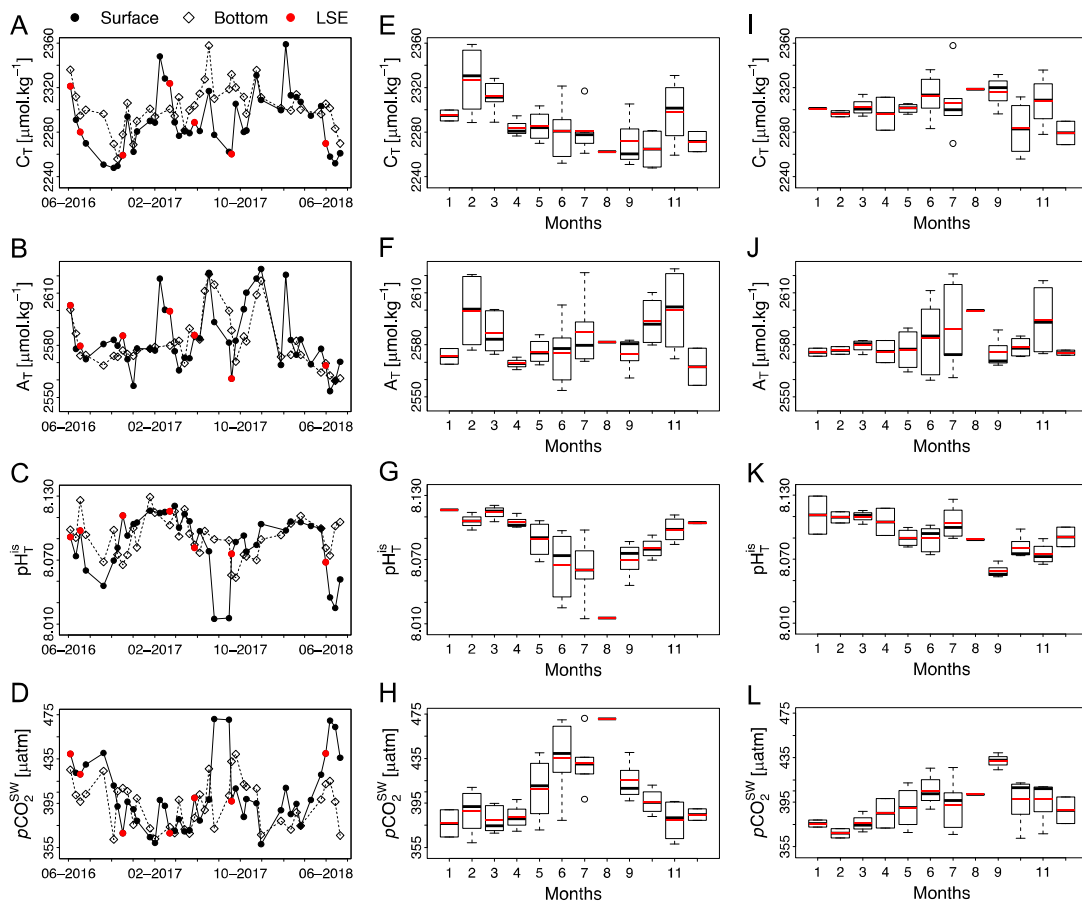
356

357 The variations in the carbonate system parameters are described in Figure 3 with the time-

358 series of C_T , A_T , pH_T^{is} and pCO_2^{SW} over the studied period (Fig.3A, 3B, 3C and 3D) and the

359 monthly mean values at surface (Fig.3E, 3F, 3G and 3H) and bottom (Fig.3I, 3J, 3K and 3L).

360



361

Figure 3. Time-series observations for seawater carbonate parameters (A, B, C, D) and box plots of pooled monthly seawater carbonate parameters at the SOLEMIO site at 1 m (black circles and solid line; Fig.3E, 3F, 3G, 3H) and at the bottom (55 m – white diamonds and dotted line; Fig.3I, 3J, 3K, 3L) from June 2016 to July 2018. In figures (A, B, C, D), red points represent Low Salinity Events (LSE). In box plots are shown the median (black line), the mean (red line), the first (Q1), and third quartiles (Q3) and data outliers (dotted lines).

362 At the surface, mean values of C_T were $2289 \mu\text{mol.kg}^{-1}$ with maximum C_T values in winter
Journal Pre-proof
363 ($2359 \mu\text{mol.kg}^{-1}$, February 2018) and minimum values in the late summer ($2248 \mu\text{mol.kg}^{-1}$,
364 October 2016). The mean C_T concentration observed at the bottom ($C_T = 2303 \mu\text{mol.kg}^{-1}$) was
365 higher than at the surface with no clear seasonal trend. Higher monthly variability of C_T is
366 observed during autumn and winter than during spring and summer (Fig.3E, 3I).

367 Mean value of A_T was similar at the bottom ($A_T = 2582 \mu\text{mol.kg}^{-1}$) to that at the surface ($A_T =$
368 $2584 \mu\text{mol.kg}^{-1}$). A_T ranged from $2554 \mu\text{mol.kg}^{-1}$ (June 2018) to $2624 \mu\text{mol.kg}^{-1}$ (November
369 2017) and did not show, at either depth, clear seasonal trends (Fig.3B, 3F and 3J). A_T presents
370 a broad variability (Fig.3F and 3J) within summer and autumn months.

371 A surface pH_T^{is} average value of 8.086 is observed with the lowest value in summer (8.015,
372 July 2017) and highest value in late winter (8.121, March 2017). Surface pH_T^{is} values present
373 a higher variability in summer than in winter (Fig.3G).

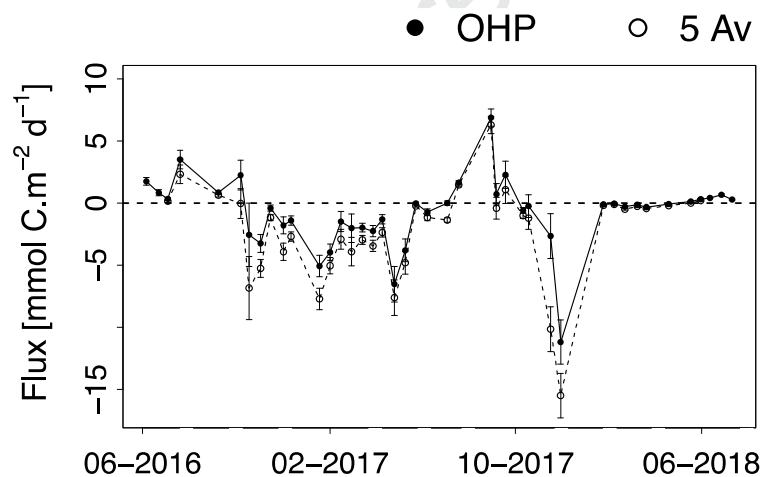
374 $p\text{CO}_2^{\text{SW}}$ ranged from $471 \mu\text{atm}$ (July 2017) to $358 \mu\text{atm}$ (November 2017) with a surface
375 mean value of $402 \mu\text{atm}$ (Table 1, Fig.3D). Large monthly variability of $p\text{CO}_2^{\text{SW}}$ is observed
376 in summer at the surface (Fig.3H). The highest $p\text{CO}_2^{\text{SW}}$ values were observed in the summer
377 months of 2017 and 2018 compared to the increase observed in 2016. Monthly means
378 distributions of $p\text{CO}_2^{\text{SW}}$ in the surface displayed a clear seasonal trend with values starting to
379 increase in late spring, reaching maximum values in summer and then a decreasing trend from
380 September onward.

381 Calcite and aragonite saturation states reveal that BoM waters were oversaturated ($\Omega > 1$)
382 with both minerals throughout the entire water column (Table 1). Mean saturation state for
383 calcite was 4.99 at the surface, and 4.67 at the bottom. For aragonite, the mean saturation state
384 was 3.23 at the surface, 3.01 at the bottom. These saturation state estimates are considered as
385 a general description of the carbonate system in the bay but will no longer be discussed in this
386 study.

387

389

390 As no $p\text{CO}_2^{\text{ATM}}$ was directly recorded over the BoM, two $p\text{CO}_2^{\text{ATM}}$ “end member” datasets
 391 are considered in order to estimate a realistic range of air-sea fluxes: the urbanised 5Av site
 392 (Fig.1), representing the higher mean $p\text{CO}_2^{\text{ATM}}$ value in the city of Marseille with the weekly
 393 mean values ranging between 399.9 and 454.3 μatm , and the OHP site (Fig.1), representing
 394 the regional background $p\text{CO}_2^{\text{ATM}}$ with values ranging between 390.4 and 416.5 μatm .
 395 The estimated mean daily air-sea CO₂ values are $-0.7 \text{ mmol C.m}^{-2}.\text{d}^{-1}$ (corresponding to -255
 396 $\text{mmol C.m}^{-2}.\text{a}^{-1}$) and $-2.2 \text{ mmol C.m}^{-2}.\text{d}^{-1}$ (corresponding to $-803 \text{ mmol C.m}^{-2}.\text{a}^{-1}$), with
 397 $p\text{CO}_2^{\text{ATM}}$ recorded at the OHP site and the 5 Av site, respectively. Fig.4 shows positive flux
 398 values in summer and spring for both atmospheric $p\text{CO}_2$ datasets used, and negative values in
 399 winter and autumn.



400

Figure 4. Time-series observations of the air-sea CO₂ flux (Flux in $\text{mmol C.m}^{-2}.\text{d}^{-1}$) with atmospheric $p\text{CO}_2$ measured at the OHP site (full circle) and at the 5 Av site (empty circle) and with $p\text{CO}_2^{\text{SW}}$ measured at the SOLEMIO site from June 2016 to July 2018. Error bars indicate errors of the associated variables of the formula used. By convention, a negative flux indicates fluxes directed from the atmosphere to the ocean, and a positive flux indicates fluxes directed from the ocean to the atmosphere.

401

402

404

405 4.1. Comparison with existing carbonate data in the Mediterranean

406

407 In the Ligurian Sea, a time-series of carbonate chemistry from the observation network
 408 MOOSE exists at the DYFAMED and ANTARES sites. Moreover, in the Bay of
 409 Villefranche-sur-Mer (Point B), a time-series of carbonate chemistry is recorded within the
 410 framework of the SOMLIT observational network (Fig.1).

411

412 *Table 2. A_T and C_T mean values in the Ligurian Sea (Point B, DYFAMED and ANTARES) and in the Bay of Mar-*
 413 *seille (SOLEMIO). Salinity-normalised changes in A_T (nA_T) and C_T (nC_T) were calculated by dividing by in situ*
 414 *salinity and multiplying by 38. SD stands for standard deviation.*

	Depth	SOMLIT (2016-2018)	Point B (2007-2016)	DYFAMED (1998-2016)	ANTARES (2010-2017)
A_T [$\mu\text{mol.kg}^{-1}$]	Surface	2584 ± 18	2555 ± 13	2568 ± 13	2563 ± 22
	Bottom	2582 ± 15	2553 ± 12	(0-50m)	(0-50m)
C_T [$\mu\text{mol.kg}^{-1}$]	Surface	2289 ± 27	2242 ± 19	2272 ± 30	2262 ± 34
	Bottom	2303 ± 20	2249 ± 17	(0-50m)	(0-50m)
nA_T [$\mu\text{mol.kg}^{-1}$]	Surface	2580 ± 30	2559 ± 17	2548 ± 8	2550 ± 18
	Bottom	2567 ± 16	2551 ± 9	(0-50m)	(0-50m)
nC_T [$\mu\text{mol.kg}^{-1}$]	Surface	2286 ± 35	2246 ± 26	2254 ± 27	2251 ± 30
	Bottom	2289 ± 19	2248 ± 17	(0-50m)	(0-50m)
Reference	/	/	Kapsenberg et al. (2017)	Coppola et al. (2018)	Lefèvre (2010)

415

416

417 When compared to Point B station data (Table 2), mean values for A_T and C_T in the BoM are
 418 higher by *ca.* $30 \mu\text{mol.kg}^{-1}$ and $50 \mu\text{mol.kg}^{-1}$, respectively. Even when normalised to salinity,
 419 this discrepancy remains. The seasonal trend observed for C_T is comparable to the seasonal
 420 trend at Point B, whereas the seasonal variation for A_T in the surface waters at this site was
 421 not observed in the BoM. The higher variability observed mostly during the summer in the

422 BoM has also been observed by Kapsenberg et al. (2017) at the Point B site and is related to
423 temperature variability.

424 For the two Ligurian open ocean time-series, the same differences with the BoM are
425 observed. A_T and C_T values were lower by *ca.* $20 \mu\text{mol.kg}^{-1}$ and $30 \mu\text{mol.kg}^{-1}$ for ANTARES,
426 and by *ca.* $15 \mu\text{mol.kg}^{-1}$ and $20 \mu\text{mol.kg}^{-1}$ for DYFAMED. Here again, when normalised to
427 salinity, higher A_T and C_T are still observed in the BoM. The Rhone River waters have higher
428 A_T concentrations which could impact the A_T values of the BoM. The LSE could be
429 associated to the inflow of Rhone River water in the BoM (see section 4.2). However, when
430 excluding LSE values from the BoM dataset, the observed differences with the three other
431 Mediterranean time-series remains (see Table 2 in supplementary material). It has to be
432 mentioned that the BoM time-series corresponds to a more recent period than the other time-
433 series. However, if an open ocean increase of $1 \mu\text{mol.kg}^{-1}.\text{a}^{-1}$ in C_T in response to the
434 atmospheric increase in CO_2 is assumed (Merlivat et al., 2018), the differences in C_T cannot be
435 explained due to time lag in sampling. In this coastal area, it is worth noting that terrestrial
436 discharges coming from the Rhone River and wastewater treatments can lead to an increase of
437 A_T as allochthonous matter (see Fig.2 in supplementary material) can be associated with non-
438 carbonate alkalinity (Hunt et al., 2011; Soetaert et al., 2007). Moreover, because A_T and C_T
439 measurements were performed simultaneously in a closed cell, the increase on A_T could lead
440 to repercussion on C_T determination (Dickson et al., 2007). Both consequences of the
441 presence of allochthonous material could affect the derived carbonate parameters. This effect,
442 certainly marginal, cannot be quantified with the present dataset.

443 The seasonal and monthly variability of the pH_T^{is} observed in the BoM shows a similar
444 dynamic to that of the Bay of Villefranche (Kapsenberg et al., 2017). For both sites this
445 dynamic is mostly driven by the temperature variations. For pCO_2^{SW} , a seasonal trend with
446 higher values during the summer period and lower values during the winter period occurs in
447 the BoM highlighting the close relationship between pCO_2^{SW} and seawater temperature. This

448 pattern has already been reported for the coastal point B site (Kapsenberg et al., 2017) but
449 also the open ocean DYFAMED site, where temperature changes can induce strong seasonal
450 variation in $p\text{CO}_2^{\text{SW}}$ values, varying between 300 and 500 μatm (Copin-Montégut et al., 2004;
451 Hood and Merlivat, 2001; Merlivat et al., 2018).

452 For the air-sea CO_2 fluxes, there are a few studies indicating that the NW MedSea is a CO_2
453 sink. In the Villefranche Bay, De Carlo et al. (2013) measured average annual fluxes (using
454 the Ho et al. (2006) formula for gas transfer velocity) of $-191 \text{ mmol C.m}^{-2}.\text{a}^{-1}$. In the Ligurian
455 Sea, at the DYFAMED site, the average annual flux (using the Wanninkhof and McGillis
456 (1999) formula for gas transfer velocity) was estimated to be $-319 \text{ mmol C.m}^{-2}.\text{a}^{-1}$ from
457 February 1998 to January 1999, and $-682 \text{ mmol C.m}^{-2}.\text{a}^{-1}$ from February 1999 to January 2000
458 (Copin-Montégut et al., 2004). In the Gulf of Trieste, Ingrosso et al. (2016) reported mean
459 annual fluxes of $-781 \pm 931 \text{ mmol C.m}^{-2}.\text{a}^{-1}$ and of $-1194 \pm 2117 \text{ mmol C.m}^{-2}.\text{a}^{-1}$ in 2012 and
460 2013, respectively. The average flux calculated at the SOLEMIO station, with $p\text{CO}_2^{\text{ATM}}$
461 recorded at the OHP site, lies between the annual fluxes recorded at these three sites. With
462 $p\text{CO}_2^{\text{ATM}}$ recorded at the 5 Av site, air-sea CO_2 fluxes are higher than those previously
463 obtained in the Ligurian Sea and closer to those estimated in the Adriatic Sea. It is worth
464 mentioning that for both studies used in this comparison (DYFAMED and Villefranche Bay),
465 $p\text{CO}_2^{\text{ATM}}$ values from Lampedusa Island are used and that at high wind speeds ($> 10 \text{ m.s}^{-1}$)
466 (Table 3), large differences between gas transfer velocity formulations appear (Ho et al.,
467 2006).

468

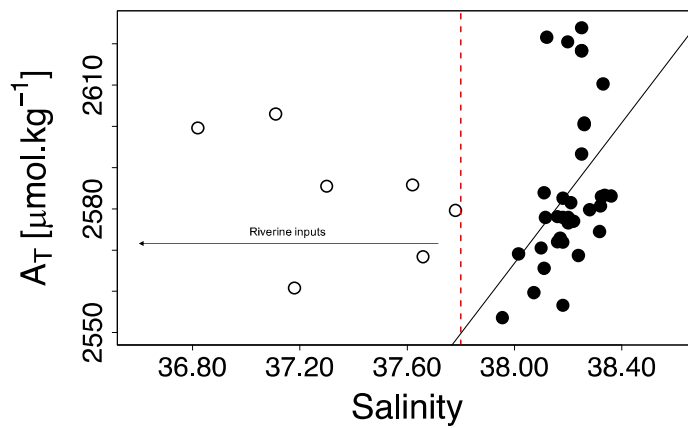
469 4.2. Influence of Low Salinity Events on A_T / Salinity relationships

470

471 A_T is considered as a conservative quantity with respect to water mixing (Wolf-Gladrow et
472 al., 2007). When biological activity is excluded, the variations of A_T should be directly related
473 to salinity changes when dilution or evaporation occurs in the ocean. In consequence, A_T
474 concentrations are generally related to salinity through a linear relationship (Copin-Montégut,

475 1993). Indeed, for sub-tropical oceans, the salinity contribution to the surface A_T variability
 Journal Pre-proof
 476 has been estimated to be greater than 80 % (Millero et al., 1998). In the MedSea, several
 477 linear relationships between A_T and salinity in the surface waters have been proposed for
 478 different sub-basins (e.g., Copin-Montégut and Bégovic, 2002; Hassoun et al., 2015; Ingrosso
 479 et al., 2016; Rivaro et al., 2010; Schneider et al., 2007). However, in the BoM, over the two-
 480 year time-series considered, no significant linear relationship between surface A_T and surface
 481 salinity has been observed (Fig.5) ($r = 0.048$, $n = 45$, p -value = 0.762).

482



483

Figure 5. A_T vs. Salinity relationship at the SOLEMIO site (1m). Red dotted line corresponds to a salinity value equal to 37.8. Empty circles represent A_T values measured at salinity under 37.8 (Low Salinity Events) and objectively excluded from the regression.

484 Based on A_T values collected over a large part of the MedSea, Schneider et al. (2007) have
 485 demonstrated that freshwater inputs from rivers affect the A_T -S relationship in the MedSea
 486 due to high A_T values of riverine inputs. This is the case for the Rhone River waters which
 487 give high alkalinity values of *ca.* 2885 $\mu\text{mol.kg}^{-1}$ (GEMSWATER data in Schneider et al.,
 488 2007).

489 The hourly surface salinity data collected from the STPS buoy network (extracted four days
 490 before, and two days after the sampling day at SOLEMIO - see methods) indicates that the
 491 seven observed LSE reported in section 3.1 are associated to the occurrence of a Rhone River

492 plume Eastward along the coast. Moreover, the offshore wind conditions (NW/N) during the
 493 prevailing period (Table 3) confirms a possible eastward extension of the Rhone plume before
 494 and during LSE observed in BoM, as demonstrated by Gangloff et al. (2017). Also, low
 495 rainfall rates have been recorded the preceding week of the LSE. This observation sustains the
 496 scenario that these LSE are due to intrusions of freshwater coming from the Rhone River in
 497 the surface of the BoM.
 498

Table 3. Distributions of salinity measured at the SOLEMIO site, the Rhone River discharge water ($m^3.h^{-1}$), the precipitation rate (mm), the wind direction ($^{\circ}$) and speed ($m.s^{-1}$) and maximum and minimum salinity values measured by the four buoys of the STPS network (see Fig.1) for the seven observed LSE.

	June 6 th , 2016	July 4 th , 2016	November 2 nd , 2016	March 15 th , 2017	May 24 th , 2017	September 6 th , 2017	May 31 th , 2018
Salinity measured	37.11	37.78	37.30	36.82	37.62	37.18	37.66
RR flow [$m^3.h^{-1}$]	2650	1400	850	2020	1200	630	2300
Precipitation [mm]	$2.16.10^{-3}$	$2.89.10^{-8}$	$1.39.10^{-2}$	$6.27.10^1$	$1.50.10^2$	$7.57.10^{-4}$	NA
Wind direction [$^{\circ}$]	174	282	NA	203	322	NA	289
Wind speed [$m.s^{-1}$]	3.46	1.84	5.66	1.99	1.84	11.19	2.44
STPS Balancelle buoy (Smin – Smax)	12.49 – 32.36	21.86 – 37.63	22.33 – 37.08	11.83 – 35.04	16.98 – 34.61	35.19 – 37.19	14.72 – 36.99
STPS Omega buoy (Smin – Smax)	19.54 – 30.29	31.42 – 34.20	NA – NA	25.79 – 35.38	33.65 – 37.30	34.08 – 37.35	NA – NA
STPS Carro buoy (Smin – Smax)	24.90 – 36.84	30.77 – 37.51	35.87 – 37.99	23.08 – 36.65	28.82 – 35.29	30.97 – 36.15	37.37 – 37.86
STPS Carry buoy (Smin – Smax)	29.38 – 37.49	31.72 – 34.28	33.36 – 38.29	32.79 – 37.93	35.45 – 37.79	33.16 – 35.97	37.24 – 37.70

499
 500
 501 When these intrusions of Rhone River water occur, the sea surface salinity is lowered (down
 502 to 36.82), but due to the elevated alkalinity values of the Rhone River, they do not induce a
 503 decrease in the A_T values (Fig.5). In consequence, the intrusion of Rhone River water during
 504 LSE can explain the deviation from the A_T -S linear relationship. Indeed, when the seven LSE
 505 values are not considered, a significant linear relationship is observed between A_T and S ($r =$
 506 0.413 , $n = 38$, p -value = 0.014).

507

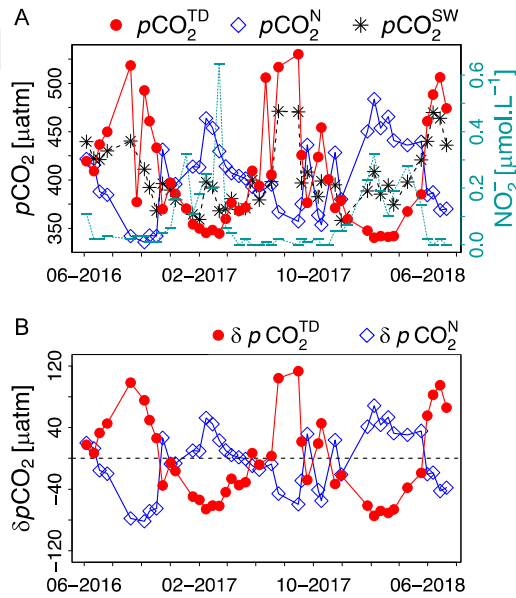
509

510 Over an annual cycle the BoM acts alternatively as a source or a sink of CO₂ due to seasonal
511 variability in the air-sea fluxes (mostly driven by the $p\text{CO}_2^{\text{SW}}$). Nevertheless, as observed in
512 other parts of the NW MedSea, on an annual scale, the BoM is a potential atmospheric CO₂
513 sink.

514 In addition to the gas solubility, air-sea CO₂ fluxes are controlled by the piston velocity and
515 the $p\text{CO}_2$ difference between seawater and atmosphere (see equation 4). The contribution of
516 these different terms to air-sea CO₂ flux variability in the BoM can be deciphered from the
517 variability of these different contributions.

518 Changes of CO₂ partial pressure in the ocean ($p\text{CO}_2^{\text{SW}}$) are due to combined effects of
519 biological and physical processes. Following the approach proposed by Takahashi et al.
520 (1993, 2002), the respective contributions of thermal and non-thermal processes on $p\text{CO}_2^{\text{SW}}$
521 have been estimated (see section 2.4.3). Fig.6A reveals consistent seasonal trends between
522 $p\text{CO}_2^{\text{SW}}$ and $p\text{CO}_2$ induced by temperature changes ($p\text{CO}_2^{\text{TD}}$). Contributions of thermal
523 ($p\text{CO}_2^{\text{TD}}$) and non-thermal processes ($p\text{CO}_2^{\text{N}}$) on $p\text{CO}_2^{\text{SW}}$ are presented in figure 6B. The
524 main variation of $p\text{CO}_2^{\text{SW}}$ occurs because of changes in surface seawater temperature, with a
525 contribution of the thermal parameter ($p\text{CO}_2^{\text{TD}}$) to the changes in $p\text{CO}_2^{\text{SW}}$ varying from +113
526 μatm (generated by warming) to -75 μatm (due to cooling) (Fig.6B), for an overall range of
527 188 μatm .

528



529

Figure 6. (A) Time-series observation for surface seawater $p\text{CO}_2^{\text{TD}}$ ($p\text{CO}_2$ changes induced by temperature (Temp-Driven); red line), surface seawater $p\text{CO}_2^{\text{N}}$ ($p\text{CO}_2$ changes induced by to non-thermal effect; blue line), surface seawater $p\text{CO}_2$ ($p\text{CO}_2^{\text{SW}}$; black line) and nitrite (NO_2^-) concentrations (green line) at the SOLEMIO site from June 2016 to July 2018. (B) Changes in $p\text{CO}_2$ that can be attributed to changes in temperature, calculated as: $\delta p\text{CO}_2^{\text{TD}} = p\text{CO}_2 - p\text{CO}_2^{\text{N}}$, and changes in $p\text{CO}_2$ that can be attributed to non-thermal effects, calculated as: $\delta p\text{CO}_2^{\text{N}} = p\text{CO}_2 - p\text{CO}_2^{\text{TD}}$. The $p\text{CO}_2^{\text{N}}$ and $p\text{CO}_2^{\text{TD}}$ used in the above equations correspond to Eqs. 2 and 3 in the text, respectively.

530 Variations in $p\text{CO}_2^{\text{SW}}$ induced by non-thermal processes ($p\text{CO}_2^{\text{N}}$) showed a regular pattern,
 531 with a seasonal maximum in winter to a minimum in summer (Fig.6A and Fig.4). The $p\text{CO}_2^{\text{N}}$
 532 variability is mainly due to biological activity, but it also includes changes due to advection,
 533 vertical diffusion and air-sea gas exchanges (De Carlo et al., 2013). The $p\text{CO}_2^{\text{N}}$ varies at the
 534 surface from +69 μatm in winter to -82 μatm in late summer (Fig.6B). In the BoM, freshwater
 535 intrusions have a crucial influence on efflorescence events which are punctual and brief (Diaz
 536 et al., 2008; Fraysse et al., 2014). The biological component being poorly represented by bi-
 537 monthly sampling of Chl-A (Fig.2 in supplementary material), $p\text{CO}_2^{\text{N}}$ could not be complete-
 538 ly related to this parameter. Variations of $p\text{CO}_2^{\text{N}}$ are partially synchronous with those of C_{T}
 539 (Fig.3A and 6A), mostly in winter. There is a more pronounced synchronous link between

540 nutrients (and in particular the nitrite concentrations) and $p\text{CO}_2^{\text{N}}$. The high concentrations of
541 nitrite in winter could be an indirect evidence of increased organic matter remineralisation by
542 heterotrophic activity. Indeed, the activity of heterotroph remineralisation releases high con-
543 tents of ammonium into the seawater (Kirchman, 2000). This accumulated ammonium might
544 then have been oxidised into nitrite through bacterial nitrification which is, furthermore, fa-
545 voured in the low light conditions found in winter (Ward, 1985). Thus, the observed nitrite
546 accumulation would result from nitrifying oxidation of ammonium (Meeder et al., 2012;
547 Zakem et al., 2018) and could indirectly sign a strengthened remineralisation of organic mat-
548 ter, especially in winter. The oxidation of organic matter by aerobic respiration producing
549 well higher contents of CO_2 than that consumed by nitrifying bacteria (Zakem et al., 2018), it
550 is then possible to observe increased quantities of NO_2^- concomitantly to increased concentra-
551 tions of C_T and $p\text{CO}_2^{\text{N}}$.

552 The increase in nitrite concentrations observed during winter, concomitant with the $p\text{CO}_2^{\text{N}}$
553 increase, might indicate that heterotrophic processes significantly contribute to the CO_2 con-
554 tent of seawater at certain periods of the year (*i.e.* winter).

555
556 These calculated $p\text{CO}_2^{\text{N}}$ and $p\text{CO}_2^{\text{TD}}$ highlight the concomitant impacts of biological activity
557 and physical processes on the $p\text{CO}_2^{\text{SW}}$ variations. During spring, depending on the nutrient
558 availability, the increase in $p\text{CO}_2$ by seawater warming is counteracted by the photosynthetic
559 uptake that simultaneously lowers C_T and nutrients stocks. Then, as the nutrient availability
560 becomes less, biological CO_2 consumption decreases in autumn and heterotrophic respiration
561 leads to an increase in the C_T and $p\text{CO}_2^{\text{N}}$ values. Moreover, during winter, seawater cooling
562 tends to decrease $p\text{CO}_2$ and this process could also be counteracted by the mixing of bottom-
563 water enriched in C_T with the deepening of the MLD (Fig.2C). The temperature in the upper
564 layer of the MedSea is increasing (Nykjaer, 2009; Vargas-Yáñez et al., 2008). Since 1997, the
565 temperature at the SOLEMIO site has increased (see section 3.1). Because of the temperature
566 predominance on the control of the $p\text{CO}_2^{\text{SW}}$ signal, this warming tendency should induce

567 higher $p\text{CO}_2^{\text{SW}}$ values in the surface layer. This could induce an increased stratification of the
Journal Pre-proof
568 water column, which could decrease the available nutrients in the euphotic zone. Therefore,
569 less $p\text{CO}_2$ could be counterbalanced by non-thermal processes, making the effect of increas-
570 ing $p\text{CO}_2^{\text{SW}}$ even stronger.

571
572 Changes of CO_2 partial pressure in the atmosphere ($p\text{CO}_2^{\text{ATM}}$) in the BoM are characterised
573 by the regional background concentration on top of which is added the effect of the urbanised
574 Marseille area. In order to highlight the anthropogenic impact of the Marseille Metropolis on
575 the BoM, two $p\text{CO}_2^{\text{ATM}}$ datasets have been used (see section 3.4). The CO_2 sink increases
576 with increasing $p\text{CO}_2^{\text{ATM}}$ values, as seen when using $p\text{CO}_2^{\text{ATM}}$ values from the 5 Av station
577 (Fig.4, dotted line). It is worth noting that in this urbanised area, the $p\text{CO}_2^{\text{ATM}}$ daily variation
578 is almost $38 \mu\text{atm}$ on average with some events exceeding $150 \mu\text{atm}$. Thus, this study shows
579 that high $p\text{CO}_2^{\text{ATM}}$, as observed in coastal anthropised areas, may increase the sink of CO_2 in
580 the surrounding marine waters.

581
582 Finally, the effect of the piston velocity on the CO_2 exchanges is highly dependent on the
583 wind speed. Indeed, at wind speeds above $7\text{-}10 \text{ m}\cdot\text{s}^{-1}$, the piston velocity increases
584 considerably. At the SOLEMIO site, wind speeds ranging between 5 and $13 \text{ m}\cdot\text{s}^{-1}$ were
585 detected during *ca.* 45 % of the time. In the BoM, the highest CO_2 in-gassing value (November
586 2017) is associated with the strongest daily wind episode ($12 \text{ m}\cdot\text{s}^{-1}$) and low $p\text{CO}_2^{\text{SW}}$ (358
587 μatm). This illustrates the potential importance of short scale events on the piston velocity of
588 the air-sea exchanges variability (Ingrosso et al., 2016). At a windy site like SOLEMIO, the
589 high $p\text{CO}_2^{\text{ATM}}$ and high wind periods could have a noticeable impact on the air-sea CO_2
590 fluxes. For example, Copin-Montégut et al. (2004) reported significant differences in the air-
591 sea CO_2 fluxes in 1998 and 1999 because of strong winds during the autumn of 1999.
592 However, Xueref-Remy et al. (2018) highlighted the fact that the amplitude of the
593 atmospheric CO_2 concentration range, and especially the maximum values, decrease

594 exponentially with wind speed because of the ventilation and dilution effects in the
Journal Pre-proof
595 atmosphere.

596 In general, at the SOLEMIO site, the time-series of the air-sea fluxes (Fig.4) displays seasonal
597 changes, for both OHP and 5 Av series, with CO₂ outgasing in summer, and ingasing in
598 winter. This observation indicates that temperature, rather than biological processes, mostly
599 drives the difference in $p\text{CO}_2$ between the ocean and the atmosphere and is certainly the main
600 contributor to the air-sea CO₂ exchange variability. Nonetheless, episodic wind events,
601 through the increase in the piston velocity, can significantly impact the air-sea CO₂ fluxes
602 over shorter time scales (daily to weekly).

603

604 4.4. Is the biological contribution to the air-sea CO₂ fluxes significant?

605

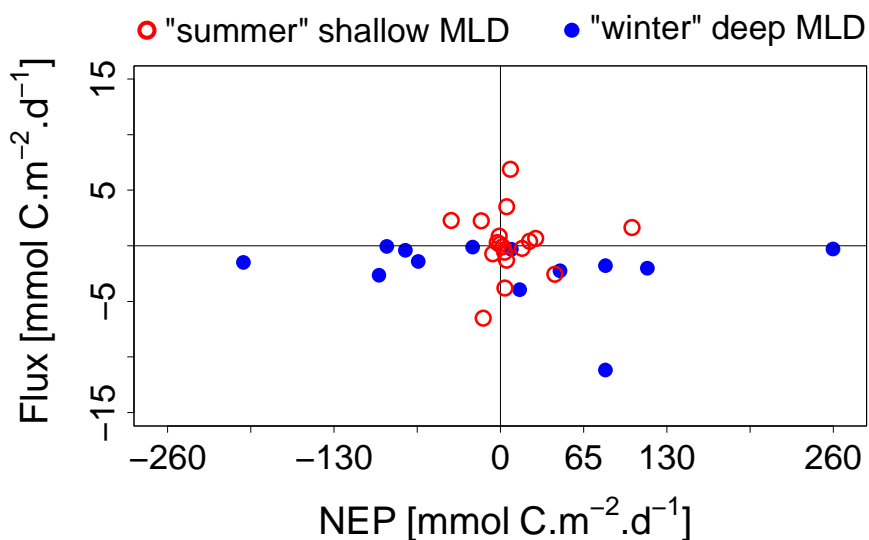
606 In a given water mass, biological processes can modify the carbonate chemistry variables and
607 thus affect the air-sea CO₂ exchanges. In the conceptual working frame proposed by Borges et
608 al. (2006), the relationship between air-sea CO₂ fluxes and net ecosystem production (NEP)
609 should be linear. In coastal environments, the physical forcing (such as coastal upwelling) and
610 net ecosystem calcification (NEC) can also modulate the carbonate chemistry properties and
611 therefore these subsequent fluxes, making the link between air-sea CO₂ fluxes and the
612 ecosystem metabolism increasingly complex.

613

614 In the BoM, no direct measurements of ecosystem productivity were available during the
615 period of this study. Oxygen derived estimations for ecosystem production based on Apparent
616 Oxygen Utilisation are not relevant in the MLD due to the short equilibration time of $p\text{O}_2$ at
617 the air-sea interface. Based on the approach proposed in Oudot (1989), a mean equilibration
618 time of $p\text{O}_2$ of 2 days is estimated for this study. To accurately estimate *in situ* metabolic rates
619 based on carbonate chemistry variations, high temporal resolution sampling over full dial
620 cycles (24h) is required. Moreover, to derive such estimates, it is assumed that the studied

621 system is a closed system, or the residence times should be considered with respect to the high
Journal Pre-proof
622 NEC estimates sensitivity to this parameter (Courtney and Andersson, 2019). No direct
623 information on water mass residence time were available for the present study. Nevertheless,
624 estimations of NEC and NEP are based on a simple assumption: the fortnightly temporal
625 variations of A_T and C_T are driven by biological processes.
626 Because the MLD constitutes one of the major factors controlling ocean primary production
627 (Sverdrup, 1953), mean values for NEC, NEP and air-sea CO_2 fluxes are reported for the two
628 defined MLD seasons in Table 1 in the supplementary material. At the SOLEMIO site, the
629 NEC daily mean value ($2.9 \pm 22.5 \text{ mmol C.m}^{-2}.\text{d}^{-1}$) suggests a net calcifying system, which is
630 in accordance with the estimated calcite and aragonite saturation states. Also, estimated NEP
631 mean values of $5.0 \pm 116.8 \text{ mmol C.m}^{-2}.\text{d}^{-1}$ and $9.0 \pm 29.2 \text{ mmol C.m}^{-2}.\text{d}^{-1}$ in winter and
632 summer (with atmospheric $p\text{CO}_2$ reference from the OHP site), respectively, suggest that the
633 BoM is a system where autotrophic processes prevail over heterotrophic processes. Over the
634 studied period, the daily NEP presents a mean value equal to $7.3 \pm 77.1 \text{ mmol C.m}^{-2}.\text{d}^{-1}$.
635 The CO_2 fluxes and trophic status of the BoM are presented in Figure 7 within the conceptual
636 frame proposed by Borges et al. (2006).

637



638

Figure 7. Air-sea CO_2 fluxes ($\text{mmol C.m}^{-2}.\text{d}^{-1}$) from the OHP site versus Net Ecosystem Production according to the Mixed Layer Depth at the SOLEMIO site from June 2016 to July 2018. By convention, positive and negative

Journal Pre-proof

NEP suggests an autotrophic status and a heterotrophic status, respectively. A negative FCO_2 sign indicates a flux directed from the atmosphere to the ocean while a positive FCO_2 sign indicates a flux directed from the ocean to the atmosphere. Data are divided into “winter” deep MLD (November to March; blue dot) and “summer” shallow MLD (April to October; red dot) in order to compare seasonal changes.

639 The mean air-sea CO_2 fluxes and NEP values are in good agreement with this conceptual
640 frame with an ecosystem where autotrophic processes are associated to a sink of CO_2 . None-
641 theless, some of the results are in contradiction to this conceptual frame: in the BoM, negative
642 NEP values (heterotrophic status) are associated with an atmospheric CO_2 sink (particularly in
643 winter).

644 In order to explain this apparent contradiction, beside the errors associated to the NEP (and
645 NEC) estimations, several reasons can be put forward: (1) In the Bay of Palma (NW MedSea),
646 Gazeau et al. (2004) reported a similar observation which was related, at least partially, to the
647 short residence time of the water mass in the bay (*ca.* 5 days). Water masses are then almost
648 immediately flushed, and biological processes have a small impact on air-sea CO_2 fluxes. In
649 the BoM, Millet et al. (2018) have measured a 5 to 10 day time-lapse for some particles to
650 reach different locations around the BoM after their release, which indicates a short residence
651 time of the water. This could partially explain the observed discrepancy with the conceptual
652 frame. (2) In addition to NEP biological contribution, calcification/dissolution can affect the
653 air-sea CO_2 fluxes. In the BoM, Bensoussan and Gattuso (2007) measured a NEC mean value
654 of $8 \text{ mmol C.m}^{-2}.\text{d}^{-1}$. Despite this estimation being an order of magnitude lower in winter in
655 this study, the importance of benthic communities in this shallow system could contribute, to
656 some extent, to the air-sea CO_2 fluxes. (3) Also, there is an order of magnitude between the
657 air-sea CO_2 exchanges and the metabolic flux intensity (Fig.7), undermining the biological
658 signature on the *in situ* carbonate chemistry. (4) Finally, temperature changes will further
659 modulate the exchange of CO_2 through its impact on pCO_2^{SW} . In the BoM, most of the pCO_2
660 changes are related to the thermal effects (see section 4.3) and are probably the main reason

661 for the apparent contradiction between the NEP and the air-sea CO₂ exchange. Thus, the sink
Journal Pre-proof
662 of atmospheric CO₂ over the BoM seems to be impacted by the physical processes with a
663 marginal contribution of biological processes. Nonetheless, considering the clear sampling
664 limitations on NEP and NEC estimations, this work underlines the need for appropriate tem-
665 poral and spatial resolution in a dedicated biological study.

666

667

Journal Pre-proof

669

670 Based on a two-year time-series, this paper presents the variability of the seawater carbonate
671 system parameters in a Mediterranean coastal site close to the second largest city in France,
672 Marseille. Based on sampling on a low temporal and spatial resolution, the air-sea CO₂ flux
673 estimations in the BoM are, on average, directed from the atmosphere to the ocean.
674 Temperature is the main force driving $p\text{CO}_2^{\text{SW}}$ variability and it also has a major control on
675 the air-sea CO₂ fluxes. As a result, temperature is the main driving force of the carbonate
676 system variability in the bay. In the case of a windy site like SOLEMIO, the high $p\text{CO}_2^{\text{ATM}}$
677 and high wind periods have a significant impact on the air-sea CO₂ fluxes during episodic
678 events through the wind effect on the gas transfer velocity. Episodic hydrodynamic events,
679 such as the LSE processes, can also modify the biogeochemical composition of the BoM.
680 However, this study shows the singularity of marine environments located at the border of
681 highly urbanised areas characterised by high amplitudes of $p\text{CO}_2^{\text{ATM}}$ due to anthropogenic
682 activity.

683 In a coastal zone like the BoM, in addition to the hydrodynamic structure of the area, this
684 manuscript highlights the need to sample concomitantly *in situ* atmospheric and oceanic
685 reservoirs. Various physical forcing affects the bay (*i.e.* Rhone River water intrusion,
686 atmospheric forcing with highly variable CO₂ concentration) on a daily and hourly scale and
687 this could not be resolved here. This study highlights the crucial need to develop integrated
688 observation systems in order to measure the variability in carbon content at a high frequency
689 in all reservoirs (ocean, atmosphere, biosphere). With an adapted temporal resolution of the
690 physical forcing, the biological CO₂ fluxes in this coastal ecosystem should also be estimated
691 in order to better understand the link between the metabolic status and the air-sea CO₂
692 exchanges. Finally, to focus on the ecosystem functioning, dedicated studies should be carried
693 out to monitor key species dynamics, with an emphasis on calcifying species (pelagic and
694 benthic), to follow the potential effect of oceanic acidification on the biodiversity.

Journal Pre-proof

697 *Data availability:* Time series data from the SOLEMIO site can be found at <http://somlit.oasu.u->
698 bordeaux.fr/mysomlit-public and are available at <http://somlit.epoc.u-bordeaux1.fr/fr/>. Carbonate system data
699 presented in this paper are available on request from the corresponding authors. Atmospheric CO₂ data can be
700 found online at <https://icos-atc.lsce.ipsl.fr/OHP> and www.atmosud.org/donnees/acces-par-station/. Requests for
701 atmospheric CO₂ data should be addressed to irene.remy-xueref@univ-amu.fr and alexandre.armengaud@airpaca.org.
702

703 *Acknowledgements:* We thank the Service d'Observation en MILieu Littoral (SOMLIT) for its permission to use
704 SOLEMIO data. We wish to thank the crewmembers of the R.V. 'Antedon II', operated by the DT-INSU, for
705 making these samplings possible. We wish to acknowledge the team of the SAM platform (Service ATmosphère
706 et océan) for their helping in field work. For seawater sample analyses, we also thank the SNAPO-CO₂ at
707 LOCEAN, Paris. The SNAPO-CO₂ service at LOCEAN is supported by CNRS-INSU and OSU Ecce-Terra.
708 Some additional data has been obtained from the MOOSE data base (<http://mistrals.sedoo.fr/MOOSE/>). We
709 acknowledge the <https://www.infoclimat.fr> for providing the Météo-France station data. We thank the two
710 anonymous reviewers for their helpful comments to improve this paper.

711 *Fundings:* This study takes part of the AMC project (Aix-Marseille Carbon Pilot Study, 2016-2019) funded and
712 performed in the framework of the Labex OT-MED (ANR-11-LABEX-0061, part of the "Investissement
713 d'Avenir" program through the A*MIDEX project ANR-11-IDEX-0001-02), funded by the French National
714 Research Agenct (ANR). The project leading to this publication has received funding from European FEDER
715 Fund under project 1166-39417.

716
717 Álvarez, M., Sanleón-Bartolomé, H., Tanhua, T., Mintrop, L., Luchetta, A., Cantoni, C., Schroeder, K. and
718 Civitarese, G., 2014. The CO₂ system in the Mediterranean Sea: A basin wide perspective. *Ocean Science*, 10
719 (1): 69-92. <https://doi.org/10.5194/os-10-69-2014>.

720
721 Aminot, A. and Kérouel, R., 2007. Dosage automatique des nutriments dans les eaux marines : méthodes en flux
722 continu. Editions Quae.

723
724 Astor, Y.M., Lorenzoni, L., Thunell, R., Varela, R., Muller-Karger, F., Troccoli, L., Taylor, G.T., Scranton, M.I.,
725 Tappa, E. and Rueda, D., 2013. Interannual variability in sea surface temperature and fCO₂ changes in the
726 Cariaco Basin. *Deep Sea Research Part II*, 93: 33-43. <https://doi.org/10.1016/j.dsr2.2013.01.002>.

727

728 Bensoussan, N. and Gattuso, J.-P., 2007. Community primary production and calcification in a NW
729 Mediterranean ecosystem dominated by calcareous macroalgae. *Marine Ecology Progress Series*, 334: 37-45.
730 <https://doi.org/10.3354/meps334037>.
731
732 Borges, A.V., Schiettecatte, L.-S., Abril, G., Delille, B. and Gazeau, F., 2006. Carbon dioxide in European
733 coastal waters. *Estuarine, Coastal and Shelf Science*, 70 (3): 375-87. <https://doi.org/10.1016/j.ecss.2006.05.046>.
734
735 Borges, A.V., Ruddick, K., Schiettecatte, L.-S. and Delille, B., 2008. Net ecosystem production and carbon
736 dioxide fluxes in the Scheldt estuarine plume. *BMC Ecology*, 8 (15): 0-15. [https://doi.org/10.1186/1472-6785-8-](https://doi.org/10.1186/1472-6785-8-15)
737 15.
738
739 Bourgeois, T., Orr, J.C., Resplandy, L., Terhaar, J., Ethé, C., Gehlen, M., and Bopp, L., 2016. Coastal-ocean
740 uptake of anthropogenic carbon. *Biogeosciences*, 13 (14): 4167-85. <https://doi.org/10.5194/bg-13-4167-2016>.
741
742 Carstensen, J. and Duarte, C.M., 2019. Drivers of pH Variability in Coastal Ecosystems. *Environmental Science*
743 *and Technology*, 53 (8): 4020-4029. <https://doi.org/10.1021/acs.est.8b03655>.
744 Clayton, T.D. and Byrne, R.H., 1993. Spectrophotometric seawater pH measurements: Total hydrogen ion
745 concentration scale calibration of m-Cresol purple and at-Sea results. *Deep Sea Research Part I: Oceanographic*
746 *Research Papers*, 40 (10): 2115-29. [https://doi.org/10.1016/0967-0637\(93\)90048-8](https://doi.org/10.1016/0967-0637(93)90048-8).
747
748 Copin-Montégut, C., 1993. Alkalinity and carbon budgets in the Mediterranean Sea. *Global Biogeochemical*
749 *Cycles*, 7 (4): 915- 925. <https://doi.org/10.1029/93GB01826>.
750
751 Copin-Montégut, C. and Bégovic, M., 2002. Distributions of carbonate properties and oxygen along the water
752 column (0–2000m) in the central part of the NW Mediterranean Sea (Dyfamed Site): Influence of winter vertical
753 mixing on air–sea CO₂ and O₂ exchanges. *Deep Sea Research Part II: Topical Studies in Oceanography*, 49
754 (11): 2049-66. [https://doi.org/10.1016/S0967-0645\(02\)00027-9](https://doi.org/10.1016/S0967-0645(02)00027-9).
755
756 Copin-Montégut, C., Bégovic, M. and Merlivat, L., 2004. Variability of the partial pressure of CO₂ on diel to
757 annual time scales in the Northwestern Mediterranean Sea. *Marine Chemistry*, 85 (3-4): 169-89.
758 <https://doi.org/10.1016/j.marchem.2003.10.005>.
759

760 Coppola, L., Diamond Riquier, E. and Carval, T., 2018. Dyfamed observatory data. SEANOE.
761 <https://doi.org/10.17882/43749> Journal Pre-proof

762

763 Courtney, T. A. and Andersson, A. J., 2019. Evaluating measurements of coral reef net ecosystem calcification
764 rates. *Coral Reefs*, 38 (5): 997-1006. <https://doi:10.1007/s00338-019-01828-2>.

765

766 De Carlo, E.H., Mousseau, L., Passafiume, O., Drupp, P.S. and Gattuso, J.-P., 2013. Carbonate chemistry and
767 air-sea CO₂ flux in a NW Mediterranean Bay over a four-year period: 2007–2011. *Aquatic Geochemistry*, 19
768 (5-6): 399-442. <https://doi.org/10.1007/s10498-013-9217-4>.

769

770 Dean, J.A. and Lange, N.A., éd. 1999. *Lange's Handbook of Chemistry*. 15. ed. McGraw-Hill Handbooks. New
771 York, NY: McGraw-Hill.

772

773 Diaz, F., Naudin, J.-J., Courties, C., Rimmelin, P. and Oriol, L., 2008. Biogeochemical and ecological function-
774 ing of the low-salinity water lenses in the region of the Rhone River freshwater influence, NW Mediterranean
775 Sea. *Continental Shelf Research*, 28 (12): 1511-1526. <https://doi/10.1016/j.csr.2007.08.009>.

776

777 Dickson, A.G., 1990. Standard potential of the reaction: $\text{AgCl(s)} + 1/2 \text{H}_2(\text{g}) = \text{Ag(s)} + \text{HCl(aq)}$, and the
778 standard acidity constant of the ion HSO_4^- in synthetic sea water from 273.15 to 318.15 K. *The Journal of*
779 *Chemical Thermodynamics*, 22 (2): 113-27. [https://doi.org/10.1016/0021-9614\(90\)90074-Z](https://doi.org/10.1016/0021-9614(90)90074-Z).

780

781 Dickson, A. G. and Millero, F., 1987. A comparison of the equilibrium constants for the dissociation of carbonic
782 acid in seawater media. *Deep Sea Research*, 34 (10): 1733–1743. [https://doi.org/10.1016/0198-0149\(87\)90021-](https://doi.org/10.1016/0198-0149(87)90021-5)
783 5.

784

785 Dickson, A.G., Sabine, C.L. et Christian, J.R., (Eds.) 2007. Guide to best practices for ocean CO₂ measurements.
786 *PICES Special Publication*, 3, 191 pp. Sidney, BC: North Pacific Marine Science Organization.

787

788 Dlugokencky, E. and Tans, P., 2019. Trends in atmospheric carbon dioxide, National Oceanic & Atmospheric
789 Administration, Earth System Research Laboratory (NOAA/ESRL), available at: [http:](http://www.esrl.noaa.gov/gmd/ccgg/trends/global.html)
790 [//www.esrl.noaa.gov/gmd/ccgg/trends/global.html](http://www.esrl.noaa.gov/gmd/ccgg/trends/global.html) (last access: November 23th 2018)

791

792 DOE, 1994. Handbook of methods for the analysis of the various parameters of the carbon dioxide system in sea
793 water. Version 2, A. G. Dickson & C. Goyet, eds. ORNL/CDIAC-74.
794
795 Doney, S.C., Fabry, V.J., Feely, R. A. and Kleypas, J.A., 2009. Ocean acidification: the other CO₂ problem.
796 *Annual Review Marine Science*, 1 (1): 169-192. <https://doi/10.1146/annurev.marine.010908.163834>.
797
798 Durrieu de Madron, X., Guieu, C., Sempéré, R., Conan, P., Cossa, D., D'Ortenzio, F., Estournel, C., Gazeau, F.,
799 Rabouille, C., Stemmann, L., Bonnet, S., Diaz, F., Koubbi, P., Radakovitch, O., Babin, M., Baklouti, M.,
800 Bancon-Montigny, C., Belviso, S., Bensoussan, N., Bonsang, B., Bouloubassi, I., Brunet, C., Cadiou, J.-F.,
801 Carlotti, F., Chami, M., Charmasson, S., Charrière, B., Dachs, J., Doxaran, D., Dutay, J.-C., Elbaz-Poulichet, F.,
802 Eléaume, M., Eyrolles, F., Fernandez, C., Fowler, S., Francour, P., Gaertner, J.C., Galzin, R., Gasparini, S.,
803 Ghiglione, J.-F., Gonzalez, J.-L., Goyet, C., Guidi, L., Guizien, K., Heimbürger, L.-E., Jacquet, S.H.M., Jeffrey,
804 W.H., Joux, F., Le Hir, P., Leblanc, K., Lefèvre, D., Lejeusne, C., Lemé, R., Loÿe-Pilot, M.-D., Mallet, M.,
805 Méjanelle, L., Mélin, F., Mellon, C., Mérigot, B., Merle, P.-L., Migon, C., Miller, W.L., Mortier, L., Mostajir,
806 B., Mousseau, L., Moutin, T., Para, J., Pérez, T., Petrenko, A., Poggiale, J.-C., Prieur, L., Pujo-Pay, M., Pulido-
807 Villena, E., Raimbault, P., Rees, A.P., Ridame, C., Rontani, J.-F., Ruiz Pino, D., Sicre, M.A., Taillandier, V.,
808 Tamburini, C., Tanaka, T., Taupier-Letage, I., Tedetti, M., Testor, P., Thébault, H., Thouvenin, B., Touratier, F.,
809 Tronczynski, J., Ulses, C., Van Wambeke, F., Vantrepotte, V., Vaz, S. and Verney, R., 2011. Marine
810 ecosystems' responses to climatic and anthropogenic forcings in the Mediterranean. *Progress in Oceanography*,
811 91 (2): 97-166. <https://doi.org/10.1016/j.pocean.2011.02.003>.
812
813 Edmond J.M., 1970. High precision determination of titration alkalinity and total carbon dioxide content of sea
814 water by potentiometric titration. *Deep Sea Research and Oceanographic Abstracts*, 17 (4): 737-50.
815 [https://doi.org/10.1016/0011-7471\(70\)90038-0](https://doi.org/10.1016/0011-7471(70)90038-0).
816
817 Fraysse, M., Pairaud, I., Ross, O.N., Faure V.M. and Pinazo C., 2014. Intrusion of Rhone river diluted water into
818 the Bay of Marseille: Generation processes and impacts on ecosystem functioning. *Journal of Geophysical*
819 *Research: Oceans*, 119 (10): 6535-56. <https://doi.org/10.1002/2014JC010022>.
820
821 Gangloff, A., Verney, R., Doxaran, D., Ody, A. and Estournel, C., 2017. Investigating Rhône river plume (Gulf
822 of Lions, France) dynamics using metrics analysis from the MERIS 300m Ocean Color Archive (2002–2012).
823 *Continental Shelf Research*, 144: 98-111. <https://doi.org/10.1016/j.csr.2017.06.024>.

825 Gatti, J., Petrenko, A., Devenon, J.-L., Leredde, Y. and Ulses, C., 2006. The Rhone River dilution zone present
826 in the North Eastern shelf of the Gulf of Lion in December 2003. *Continental Shelf Research*, 26 (15):
827 1794-1805. <https://doi.org/10.1016/j.csr.2006.05.012>.

828

829 Gattuso, J.-P., Frankignoulle, M. and Wollast, R., 1998. Carbon and carbonate metabolism in coastal aquatic
830 ecosystems. *Annual Review of Ecology and Systematics*, 29 (1): 405-34.
831 <https://doi.org/10.1146/annurev.ecolsys.29.1.405>.

832

833 Gazeau, F., Duarte, C.M., Gattuso, J.-P., Barrón, C., Navarro, N., Ruíz, S., Prairie, Y.T., Calleja, M., Delille, B.,
834 Frankignoulle, M. and Borges, A.V., 2004. Whole-system metabolism and CO₂ fluxes in a Mediterranean Bay
835 dominated by seagrass beds (Palma Bay, NW Mediterranean). *Biogeosciences Discussions*, 1 (1): 755-802.
836 <https://doi.org/10.5194/bgd-1-755-2004>.

837

838 Gruber, N., Clement, D., Carter, B.R., Feely, R.A., Van Heuven, S., Hoppema, M., Ishii, M., Key, R.M., Kozyr,
839 A., Lauvset, S.K., Lo Monaco, C., Mathis, J.T., Murata, A., Olsen, A., Perez, F.F., Sabine, C.L., Tanhua, T. and
840 Wanninkhof, R., 2019. The oceanic sink for anthropogenic CO₂ from 1994 to 2007. *Science*, 363 (6432):1193-
841 1199. <https://doi.org/10.1126/science.aau5153>.

842

843 Hassoun, A.E.R., Gemayel, E., Krasakopoulou, E., Goyet, C., Saab, M.A.-A., Ziveri, P., Touratier, F., Guglielmi
844 V. and Falco, C., 2015. Modeling of the Total Alkalinity and the Total Inorganic Carbon in the Mediterranean
845 Sea. *Journal of Water Resources and Ocean Science*, 4 (1): 24. <https://doi.org/10.11648/j.wros.20150401.14>.

846

847 Ho, D.T., Law, C.S., Smith, M.J., Schlosser, P., Harvey M. and Hill, P., 2006. Measurements of air-sea gas
848 exchange at high wind speeds in the Southern Ocean: Implications for global parameterizations. *Geophysical
849 Research Letters*, 33 (16). <https://doi.org/10.1029/2006GL026817>.

850

851 Hood, E.M. and Merlivat, L., 2001. Annual to interannual variations of CO₂ in the Northwestern Mediterranean
852 Sea: Results from hourly measurements made by CARIOCA buoys, 1995-1997. *Journal of Marine Research*, 59
853 (1): 113-31. <https://doi.org/10.1357/002224001321237399>.

854

855 Huang, Y.-H., Lee, C.-L., Chung, C.-Y., H, S.-C. and Lin, H.-J., 2015. Carbon budgets of multispecies seagrass
856 beds at Dongsha Island in the South China Sea. *Marine Environmental Research*, 106 (1): 92-102.
857 <https://doi.org/10.1016/j.marenvres.2015.03.004>.
858
859 Hunt, C. W., Salisbury, J. E. and Vandemark, D., 2011. Contribution of non-carbonate anions to total alkalinity
860 and overestimation of $p\text{CO}_2$ in New England and New Brunswick rivers. *Biogeosciences*, 8 (10): 3069–3076,
861 <https://doi.org/10.5194/bg-8-3069-2011>, 2011.
862
863 Ingrosso, G., Giani, M., Comici, C., Kralj, M., Piacentino, S., De Vittor, C. and Del Negro, P., 2016. Drivers of
864 the carbonate system seasonal variations in a Mediterranean gulf. *Estuarine, Coastal and Shelf Science*, 168: 58-
865 70. <http://dx.doi.org/10.1016/j.ecss.2015.11.001>.
866
867 IPCC, 2018: Summary for Policymakers. In: Global Warming of 1.5°C. An IPCC Special Report on the impacts
868 of global warming of 1.5°C above pre-industrial levels and related global greenhouse gas emission pathways, in
869 the context of strengthening the global response to the threat of climate change, sustainable development, and
870 efforts to eradicate poverty [Masson-Delmotte, V., P. Zhai, H.-O. Pörtner, D. Roberts, J. Skea, P.R. Shukla, A.
871 Pirani, Moufouma-Okia, C. Péan, R. Pidcock, S. Connors, J.B.R. Matthews, Y. Chen, X. Zhou, M.I. Gomis, E.
872 Lonnoy, Maycock, M. Tignor, and T. Waterfield (eds.)]. World Meteorological Organization, Geneva,
873 Switzerland, 32 pp.
874
875 Kapsenberg, L., Alliouane, S., Gazeau, F., Mousseau, L. and Gattuso, J.-P., 2017. Coastal ocean acidification
876 and increasing total alkalinity in the Northwestern Mediterranean Sea. *Ocean Science*, 13 (3): 411-26.
877 <https://doi.org/10.5194/os-13-411-2017>.
878
879 Kirchman, D.L., 2000. Uptake and regeneration of inorganic nutrients by marine heterotrophic bacteria. In:
880 Kirchman, D.L. (Ed.), *Microbial Ecology of the Oceans*. Wiley, pp. 261-288.
881
882 Kirkman, H. and Reid, D.D., 1979. A study of the role of the seagrass *Posidonia australis* in the carbon budget
883 of an estuary. *Aquatic Botany*, 7: 173-183. [https://doi.org/10.1016/0304-3770\(79\)90020-2](https://doi.org/10.1016/0304-3770(79)90020-2).
884

885 Laruelle, G. G., Lauerwald, R, Pfeil, B. and Regnier, P., 2014. Regionalized global budget of the CO₂ exchange
886 at the air-water interface in continental shelf seas. *Global Biogeochemical Cycles*, 28 (11): 1199-1214.
887 <https://doi.org/10.1002/2014GB004832>.
888
889 Lefèvre, D., 2010. MOOSE (ANTARES). <https://doi.org/10.18142/233>.
890
891 Louanchi, F., Boudjakdji, M. and Nacef, L., 2009. Decadal changes in surface carbon dioxide and related
892 variables in the Mediterranean Sea as inferred from a coupled data-diagnostic model approach. *ICES Journal of*
893 *Marine Science*, 66 (7): 1538-46. <https://doi.org/10.1093/icesjms/fsp049>.
894
895 Meeder, E., Mackey, K.R.M, Paytan, A., Shaked, Y., Iluz, D., Stambler, N., Rivlin, T., Post, A.F. and Lazar, B.,
896 2012. Nitrite dynamics in the open ocean - clues from seasonal and diurnal variations. *Marine Ecology Progress*
897 *Series*, 453: 11-26. <https://doi.org/10.3354:meps09525>.
898
899 Mehrbach, C., Culberson, C. H., Hawley, J. E., and Pytkowicz, R. M., 1973. Measurement of the apparent disso-
900 ciation constants of carbonic acid in seawater at atmospheric pressure. *Limnology and Oceanography*, 18
901 (6):897-907.<https://doi.org/10.4319/lo.1973.18.6.0897>.
902
903 Merlivat, L., Boutin, J., Antoine, D., Beaumont, L., Golbol, M. and Vellucci, V., 2018. Increase of dissolved
904 inorganic carbon and decrease in pH in near-surface waters in the Mediterranean Sea during the past two
905 decades. *Biogeosciences*, 15 (18): 5653 - 5662. <https://doi.org/10.5194/bg-15-5653-2018>.
906
907 Millero, F.J., 1995. Thermodynamics of the carbon dioxide system in the oceans. *Geochimica et Cosmochimica*
908 *Acta*, 59 (4): 661-77. [https://doi.org/10.1016/0016-7037\(94\)00354-O](https://doi.org/10.1016/0016-7037(94)00354-O).
909
910 Millero, F.J., Lee K. and Roche, M., 1998. Distribution of alkalinity in the surface waters of the major oceans.
911 *Marine Chemistry*, 60 (1-2): 111-30. [https://doi.org/10.1016/S0304-4203\(97\)00084-4](https://doi.org/10.1016/S0304-4203(97)00084-4).
912
913 Millet, B., Pinazo, C., Banaru, D., Pagès, R., Guiart, P. and Pairaud, I., 2018. Unexpected spatial impact of
914 treatment plant discharges induced by episodic hydrodynamic events: Modelling lagrangian transport of fine
915 particles by Northern Current intrusions in the Bays of Marseille (France). Édité par João Miguel Dias. *PLoS*
916 *ONE*, 13 (4): e0195257. <https://doi.org/10.1371/journal.pone.0195257>.

917

918 Monterey, G., and Levitus, S., 1997. Seasonal variability of mixed layer depth for the world ocean. NOAA Atlas
919 NESDIS 14, U. S. Govt. Printing Office.

920

921 Nykjaer, L., 2009. Mediterranean Sea surface warming 1985-2006. *Climate Research*, 39 (1):11-17.
922 <https://doi.org/10.3354/cr00794>.

923

924 Olafsson, J., Olafsdottir, S.R., Benoit-Cattin, A. and Takahashi, T., 2010. The Irminger Sea and the Iceland Sea
925 time series measurements of sea water carbon and nutrient chemistry 1983–2008. *Earth System Science Data*, 2
926 (1): 99-104. <https://doi.org/10.5194/essd-2-99-2010>.

927

928 Oudot, C., 1989. O₂ and CO₂ balances approach for estimating production in the mixed layer of the tropical
929 Atlantic Ocean (Guinea Dome area). *Journal of Marine Research*, 47, 385–409.

930

931 Petrenko, A., 2003. Variability of circulation features in the Gulf of Lion NW Mediterranean Sea. Importance of
932 inertial currents. *Oceanologica Acta*, 26 (4): 323-38. [https://doi.org/10.1016/S0399-1784\(03\)00038-0](https://doi.org/10.1016/S0399-1784(03)00038-0).

933

934 Pierrot, D., Lewis, E., and Wallace, D. W. R., 2006. MS Excel Program Developed for CO₂ System
935 Calculations, Tech. rep., Carbon Dioxide Inf. Anal. Cent., Oak Ridge Natl. Lab., US DOE, Oak Ridge, Tenn.

936

937 Pont, D., Simonnet, J.-P. and Walter, A.V., 2002. Medium-term changes in suspended sediment delivery to the
938 ocean: Consequences of catchment heterogeneity and river management (Rhône river, France). *Estuarine,
939 Coastal and Shelf Science*, 54 (1): 1-18. <https://doi.org/10.1006/ecss.2001.0829>.

940

941 Rivaro, P., Messa, R., Massolo, S. and Frache, R., 2010. Distributions of carbonate properties along the water
942 column in the Mediterranean Sea: Spatial and temporal variations. *Marine Chemistry*, 121 (1-4): 236-45.
943 <https://doi.org/10.1016/j.marchem.2010.05.003>.

944

945 Schneider, A., Wallace, D.W.R. and Körtzinger, A., 2007. Alkalinity of the Mediterranean Sea: Alkalinity of the
946 Mediterranean Sea. *Geophysical Research Letters*, 34 (15): L15608. <https://doi.org/10.1029/2006GL028842>.

947

948 Soetaert, K., Hofmann, A.F., Middelburg, J.J., Meysman, F.J.R. and Greenwood, J., 2007. The effect of biogeo-
949 chemical processes on pH. *Marine Chemistry*, 105 (1): 30-51. <https://doi.org/10.1016/j.marchem.2006.12.01>.
950
951 Sokal, R.R. and Rohlf, F.J., 1969. *Biometry. The principles and practices of statistics in biological research*. 2nd
952 Edition, W.H. Freeman, San Francisco.
953
954 Suzuki, A. and Kawahata, H., 2003. Carbon budget of coral reef systems: an overview of observations in fring-
955 ing reefs, barrier reefs and atolls in the Indo-Pacific regions. *Tellus B: Chemical and Physical Meteorology*, 55
956 (2): 428-444. <https://doi.org/10.1034/j.1600-0889.2003.01442.x>.
957
958 Sverdrup, H. U, 1953. On conditions for the vernal blooming of phytoplankton. *ICES Journal of Marine Science*,
959 18 (3):287-295. <https://doi.org/10.1093/icesjms/18.3.287>.
960
961 Taillandier, V., D'Ortenzio, F. and Antoine, D., 2012. Carbon fluxes in the mixed layer of the Mediterranean Sea
962 in the 1980s and the 2000s. *Deep Sea Research Part I: Oceanographic Research Papers*, 65: 73-84.
963 <https://doi.org/10.1016/j.dsr.2012.03.004>.
964
965 Takahashi, T., Olafsson, J., Goddard, J.G., Chipman, D.W. and Sutherland, S.C., 1993. Seasonal variation of
966 CO₂ and nutrients in the high-latitude surface oceans: A comparative study. *Global Biogeochemical Cycles*, 7
967 (4): 843-78. <https://doi.org/10.1029/93GB02263>.
968
969 Takahashi, T., Sutherland, S.C., Sweeney, C., Poisson, A., Metzl, N., Tilbrook, B., Bates, N., Wanninkhof, R.,
970 Feely, R.A., Sabine, C., Olafsson, J. and Nojiri, Y., 2002. Global sea-air CO₂ flux based on climatological
971 surface ocean pCO₂, and seasonal biological and temperature effects. *Deep Sea Research Part II: Topical*
972 *Studies in Oceanography*, 49 (9-10): 1601-22. [https://doi.org/10.1016/S0967-0645\(02\)00003-6](https://doi.org/10.1016/S0967-0645(02)00003-6).
973
974 Touratier, F. and Goyet, C., 2009. Decadal evolution of anthropogenic CO₂ in the north western Mediterranean
975 Sea from the mid-1990s to the mid-2000s. *Deep Sea Research Part I*, 56 (10): 1708-1716.
976 <https://doi.org/10.1016/j.dsr.2009.05.015>.
977
978 Xueref-Remy, I., Dieudonné, E., Vuillemin, C., Lopez, M., Lac, C., Schmidt, M., Delmotte, M., Chevallier F.,
979 Ravetta, F., Perrussel, O., Ciais, P., Bréon, F.-M., Broquet, G., Ramonet, M., Spain, T.G. and Ampe, C., 2018.

- 980 Diurnal, synoptic and seasonal variability of atmospheric CO₂ in the Paris megacity area. *Atmospheric*
981 *Chemistry and Physics*, 18 (5): 3335-62. <https://doi.org/10.5194/acp-18-3335-2018>.
- 982
- 983 Vargas-Yáñez, M., García, J., Salat, J., García-Martí, M.C., Pascual, J. and Moya, F., 2008. Warming trends and
984 decadal variability in the Western Mediterranean shelf. *Global and Planetary Change*, 63 (2-3): 177-184.
985 <https://doi.org/10.1016/j.gloplacha.2007.09.001>.
- 986
- 987 Wanninkhof, R., Park G.H., Takahashi T., Sweeney C., Feely R., Nojiri Y., Gruber N., Doney, S.C., McLinley,
988 G.A., Lenton, A., Le Quéré, C., Heinze, C., Schwinger, J., Graven, H. and Khatiwala, S., 2013. Global ocean
989 carbon uptake: magnitude, variability and trends. *Biogeosciences*, 10 (3): 1983-2000.
- 990
- 991 Wanninkhof, R., 2014. Relationship between wind speed and gas exchange over the ocean revisited. *Limnology*
992 *and Oceanography: Methods*, 12 (6):351-362. <https://doi.org/10.4319/lom.2014.12.351>.
- 993
- 994 Wanninkhof, R. and McGillis, W.R., 1999. A cubic relationship between air-Sea CO₂ exchange and wind speed.
995 *Geophysical Research Letters*, 26 (13): 1889-92. <https://doi.org/10.1029/1999GL900363>.
- 996
- 997 Weiss, R.F., 1974. Carbon dioxide in water and seawater: The solubility of a non-ideal gas. *Marine Chemistry*, 2
998 (3): 203-15. [https://doi.org/10.1016/0304-4203\(74\)90015-2](https://doi.org/10.1016/0304-4203(74)90015-2).
- 999
- 1000 Ward, B., 1985. Light and substrate concentration relationships with marine ammonium assimilation and oxida-
1001 tion rates. *Marine Chemistry*, 16 (4): 301-316. [https://doi.org/10.1016/0304-4203\(85\)90052-0](https://doi.org/10.1016/0304-4203(85)90052-0).
- 1002
- 1003 Ware, J.R., Smith, S.V. and Reaka-Kudla, M.L., 1992. Coral reefs: sources or sinks of atmospheric CO₂? *Coral*
1004 *Reefs*, 11 (3): 127-130. <https://doi.org/10.1007/BF00255465>.
- 1005
- 1006 Wolf-Gladrow, D.A., Zeebe, R.E., Klaas, C., Körtzinger, A. and Dickson, A.G., 2007. Total alkalinity: The
1007 explicit conservative expression and its application to biogeochemical processes. *Marine Chemistry*, 106 (1-2):
1008 287-300. <https://doi.org/10.1016/j.marchem.2007.01.006>.
- 1009
- 1010 Wollast R. 1998. Evaluation and comparison of the global carbon cycle in the coastal zone and in the open
1011 ocean. In: Brink, K.H., Robinson, A.R. (Eds.), *The Sea*. John Wiley & Sons, New York., 213-252.

1012

1013 Yao, W., Liu, X. and Byrne, R.H., 2007. Impurities in indicators used for spectrophotometric seawater pH
 1014 measurements: Assessment and remedies. *Marine Chemistry*, 107 (2): 167-172.
 1015 <https://doi.org/10.1016/j.marchem.2007.06.012>.

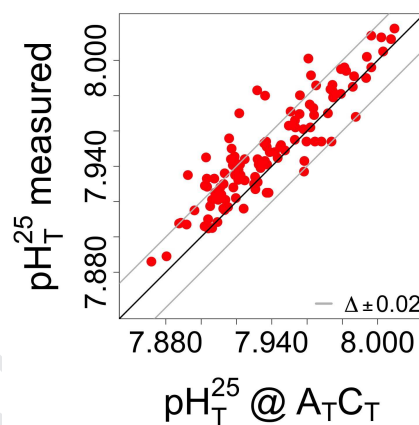
1016

1017 Zakem, E.J., Al-Haj, A., Church, M.J., Van Dijken, G.L., Dutkiewicz, S., Foster, S.Q., Fulweiler, R.W., Mills,
 1018 M.M. and Folows, M.J., 2018. Ecological control of nitrite in the upper ocean. *Nature Communications*, 9
 1019 (1206): 1-13. <https://doi.org/10.1038/s41467-018-03553-w>.

1020

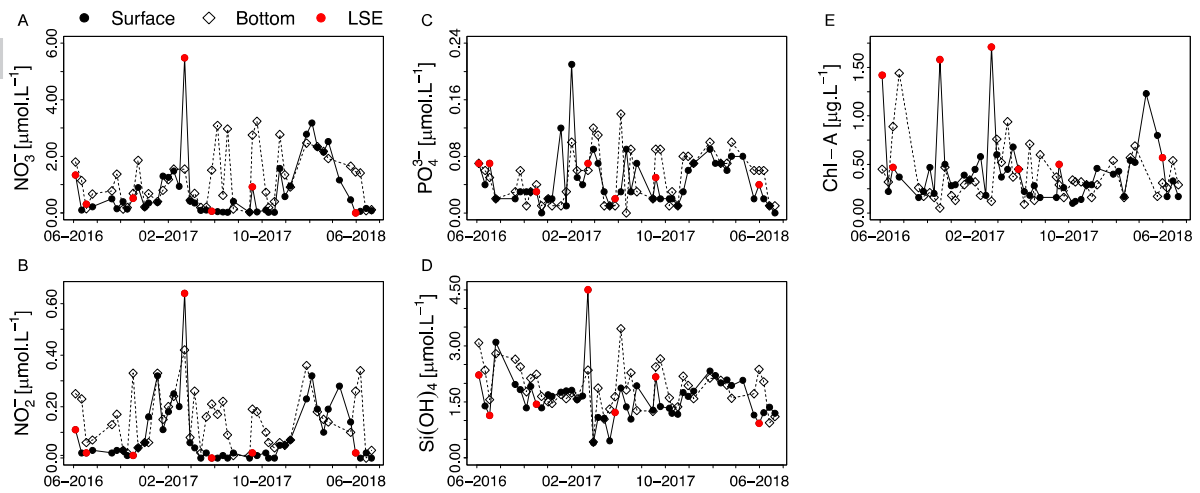
1021 Supplementary material

1022



1023

Figure 1. pH_T normalised at 25°C (pH_T^{25}) measured by spectrophotometry versus pH_T normalised at 25°C calculated from A_T and C_T variables. Black line represents a slope equal to 1, while grey lines indicates a Δ (pH_T^{25} measured – pH_T^{25} @ $A_T C_T$) equal to ± 0.02 .



1024

Figure 2. Time-series observations for nitrate (NO_3^- ; A), nitrite (NO_2^- ; B), phosphate (PO_4^{3-} ; C), orthosilicic acid ($\text{Si}(\text{OH})_4$; D) and chlorophyll A (Chl-A; E) concentrations at the SOLEMIO site at 1 m (black circles and solid line) and at the bottom (55 m – white diamonds and dotted line) from June 2016 to July 2018. In figures (A, B, C, D), red points represent low salinity events (LSE). Chl-A was extracted using 90% acetone and analysed with the fluorimetric method developed by Yentsch and Menzel (1963) [Yentsch, C.S. and Menzel, D.W., 1963. A method for the determination of phytoplankton chlorophyll and phaeophytin by fluorescence. *Deep-Sea Res.*, 10: 221-231]

1025 Table 1. Average Net Ecosystem Calcification (NEC; $\text{mmol C.m}^{-2}.\text{d}^{-1}$), Net Ecosystem Production (NEP; mmol
 1026 $\text{C.m}^{-2}.\text{d}^{-1}$) and air-sea CO_2 flux (FCO_2 ; $\text{mmol C.m}^{-2}.\text{d}^{-1}$) from June 2016 to July 2018 at the SOLEMIO site ac-
 1027 cording to atmospheric pCO_2 values recorded at the OHP site and at the 5 Av site. Data are divided into “win-
 1028 ter” deep MLD (November to March) and “summer” shallow MLD (April to October) in order to compare sea-
 1029 sonal changes. By convention, negative and positive values of NEC indicate net dissolution and precipitation of
 1030 CaCO_3 , respectively, a positive NEP suggests an autotrophic status for the area studied while a negative NEP
 1031 indicates a heterotrophic status and a negative sign FCO_2 indicates a flux directed from the atmosphere to the
 1032 ocean. SD stands for standard deviation. LSE data have been removed from these calculations.

	OHP atmospheric pCO_2			5 Av atmospheric pCO_2		
	NEC ($\text{mmol C.m}^{-2}.\text{d}^{-1}$)	NEP ($\text{mmol C.m}^{-2}.\text{d}^{-1}$)	FCO_2 ($\text{mmol C.m}^{-2}.\text{d}^{-1}$)	NEC ($\text{mmol C.m}^{-2}.\text{d}^{-1}$)	NEP ($\text{mmol C.m}^{-2}.\text{d}^{-1}$)	FCO_2 ($\text{mmol C.m}^{-2}.\text{d}^{-1}$)
Summer	4.4 ± 11.5	9.0 ± 29.2	0.2 ± 2.7	4.4 ± 11.5	8.7 ± 32.8	-0.9 ± 3.4
Winter	0.7 ± 32.8	5.0 ± 116.8	-2.2 ± 2.9	0.7 ± 32.8	6.7 ± 116.7	-3.9 ± 4.3

1033

Table 2. A_T and C_T mean values in the BoM (SOLEMIO) without LSE values. Salinity-normalised changes in nA_T and nC_T were calculated by dividing by in situ salinity and multiplying by 38. SD stands for standard deviation.

	Depth	$A_T \text{ } \emptyset \text{ LSE } [\mu\text{mol.kg}^{-1}]$	$C_T \text{ } \emptyset \text{ LSE } [\mu\text{mol.kg}^{-1}]$	$nA_T \text{ } \emptyset \text{ LSE } [\mu\text{mol.kg}^{-1}]$	$nC_T \text{ } \emptyset \text{ LSE } [\mu\text{mol.kg}^{-1}]$
SOLEMIO (2016 – 2018)	Surface	2584 ± 19	2289 ± 17	2570 ± 17	2277 ± 27
	Bottom	2582 ± 17	2302 ± 20	2567 ± 17	2288 ± 20

Journal Pre-proof

Table 1. Time-series analyses on seawater carbonate chemistry at the SOLEMIO site for temperature (Temp.), salinity, pH_T measured in situ (pH_{Tis}), total alkalinity (A_T), dissolved inorganic carbon (C_T), partial pressure of CO_2 (pCO_2), nitrate (NO_3^-), nitrite (NO_2^-), phosphate (PO_4^{3-}), orthosilicic acid ($SiOH_4$), calcite (Ω_C) and aragonite (Ω_A) saturation states, from June 2016 to July 2018, at 1 m and at the bottom (55 m). SD stands for standard deviation. DL stands for Detection Limit.

SURFACE	Mean \pm SD	Min. – Max	BOTTOM	Mean \pm SD	Min. – Max
Temp. [$^{\circ}C$]	16.90 \pm 3.16	12.94 – 23.42	Temp. [$^{\circ}C$]	14.65 \pm 1.33	12.93 – 19.71
Salinity	38.07 \pm 0.34	36.82 – 38.36	Salinity	38.22 \pm 0.06	38.06 – 38.33
pH_{Tis}	8.086 \pm 0.028	8.015 – 8.121	pH_{Tis}	8.091 \pm 0.018	8.053 – 8.129
A_T [$\mu\text{mol.kg}^{-1}$]	2584 \pm 18	2554 – 2624	A_T [$\mu\text{mol.kg}^{-1}$]	2582 \pm 15	2560 – 2621
C_T [$\mu\text{mol.kg}^{-1}$]	2289 \pm 27	2248 – 2359	C_T [$\mu\text{mol.kg}^{-1}$]	2303 \pm 20	2256 – 2358
pCO_2 [μatm]	402 \pm 31	358 – 471	pCO_2 [μatm]	394 \pm 21	362 – 439
NO_3^- [$\mu\text{mol.L}^{-1}$]	0.78 \pm 1.07	<DL – 5.48	NO_3^- [$\mu\text{mol.L}^{-1}$]	1.16 \pm 0.94	0.03 – 3.5
NO_2^- [$\mu\text{mol.L}^{-1}$]	0.09 \pm 0.12	<DL – 0.64	NO_2^- [$\mu\text{mol.L}^{-1}$]	0.14 \pm 0.11	0.01 – 0.42
PO_4^{3-} [$\mu\text{mol.L}^{-1}$]	0.05 \pm 0.04	<DL – 0.21	PO_4^{3-} [$\mu\text{mol.L}^{-1}$]	0.05 \pm 0.04	<DL – 0.14
$SiOH_4$ [$\mu\text{mol.L}^{-1}$]	1.63 \pm 0.65	0.41 – 4.50	$SiOH_4$ [$\mu\text{mol.L}^{-1}$]	1.86 \pm 0.59	0.43 – 3.46
Ω_C	4.99 \pm 0.33	4.44 – 5.64	Ω_C	4.67 \pm 0.23	4.23 – 5.29
Ω_A	3.23 \pm 0.24	2.85 – 3.70	Ω_A	3.01 \pm 0.16	2.72 – 3.45

Table 2. A_T and C_T mean values in the Ligurian Sea (Point B, DYFAMED and ANTARES) and in the Bay of Marseille (SOLEMIO). Salinity-normalised changes in A_T (nA_T) and C_T (nC_T) were calculated by dividing by in situ salinity and multiplying by 38. SD stands for standard deviation.

	Depth	SOMLIT (2016-2018)	Point B (2007-2016)	DYFAMED (1998-2016)	ANTARES (2010-2017)
A_T [$\mu\text{mol.kg}^{-1}$]	Surface	2584 \pm 18	2555 \pm 13	2568 \pm 13	2563 \pm 22
	Bottom	2582 \pm 15	2553 \pm 12	(0-50m)	(0-50m)
C_T [$\mu\text{mol.kg}^{-1}$]	Surface	2289 \pm 27	2242 \pm 19	2272 \pm 30	2262 \pm 34
	Bottom	2303 \pm 20	2249 \pm 17	(0-50m)	(0-50m)
nA_T [$\mu\text{mol.kg}^{-1}$]	Surface	2580 \pm 30	2559 \pm 17	2548 \pm 8	2550 \pm 18
	Bottom	2567 \pm 16	2551 \pm 9	(0-50m)	(0-50m)
nC_T [$\mu\text{mol.kg}^{-1}$]	Surface	2286 \pm 35	2246 \pm 26	2254 \pm 27	2251 \pm 30
	Bottom	2289 \pm 19	2248 \pm 17	(0-50m)	(0-50m)
Reference	/	/	Kapsenberg et al. (2017)	Coppola et al. (2018)	Lefèvre (2010)

Table 3. Distributions of salinity measured at the SOLEMIO site, the Rhone River discharge water ($m^3.h^{-1}$), the precipitation rate (mm), the wind direction ($^{\circ}$) and speed ($m.s^{-1}$) and maximum and

minimum salinity values measured by the four buoys of the STPS network (see Fig.1) for the seven observed LSE.

	June 6 th , 2016	July 4 th , 2016	November 2 nd , 2016	March 15 th , 2017	May 24 th , 2017	September 6 th , 2017	May 31 th , 2018
Salinity measured	37.11	37.78	37.30	36.82	37.62	37.18	37.66
RR flow [m ³ .h ⁻¹]	2650	1400	850	2020	1200	630	2300
Precipitation [mm]	2.16.10 ⁻³	2.89.10 ⁻⁸	1.39.10 ⁻²	6.27.10 ¹	1.50.10 ²	7.57.10 ⁻⁴	NA
Wind direction [°]	174	282	NA	203	322	NA	289
Wind speed [m.s ⁻¹]	3.46	1.84	5.66	1.99	1.84	11.19	2.44
STPS Balancelle buoy (Smin – Smax)	12.49 – 32.36	21.86 – 37.63	22.33 – 37.08	11.83 – 35.04	16.98 – 34.61	35.19 – 37.19	14.72 – 36.99
STPS Omega buoy (Smin – Smax)	19.54 – 30.29	31.42 – 34.20	NA – NA	25.79 – 35.38	33.65 – 37.30	34.08 – 37.35	NA – NA
STPS Carro buoy (Smin – Smax)	24.90 – 36.84	30.77 – 37.51	35.87 – 37.99	23.08 – 36.65	28.82 – 35.29	30.97 – 36.15	37.37 – 37.86
STPS Carry buoy (Smin – Smax)	29.38 – 37.49	31.72 – 34.28	33.36 – 38.29	32.79 – 37.93	35.45 – 37.79	33.16 – 35.97	37.24 – 37.70

Table1. (Supp). Average Net Ecosystem Calcification (NEC; mmol C.m⁻².d⁻¹), Net Ecosystem Production (NEP; mmol C.m⁻².d⁻¹) and air-sea CO₂ flux (FCO₂; mmol C.m⁻².d⁻¹) from June 2016 to July 2018 at the SOLEMIO site according to atmospheric pCO₂ values recorded at the OHP site and at the 5 Av site. Data are divided into “winter” deep MLD (November to March) and “summer” shallow MLD (April to October) in order to compare seasonal changes. By convention, negative and positive values of NEC indicate net dissolution and precipitation of CaCO₃, respectively, a positive NEP suggests an autotrophic status for the area studied while a negative NEP indicates a heterotrophic status and a negative sign FCO₂ indicates a flux directed from the atmosphere to the ocean. SD stands for standard deviation. LSE data have been removed from these calculations.

	OHP atmospheric pCO ₂			5 Av atmospheric pCO ₂		
	NEC (mmol C.m ⁻² .d ⁻¹)	NEP (mmol C.m ⁻² .d ⁻¹)	FCO ₂ (mmol C.m ⁻² .d ⁻¹)	NEC (mmol C.m ⁻² .d ⁻¹)	NEP (mmol C.m ⁻² .d ⁻¹)	FCO ₂ (mmol C.m ⁻² .d ⁻¹)
Summer	4.4 ± 11.5	9.0 ± 29.2	0.2 ± 2.7	4.4 ± 11.5	8.7 ± 32.8	-0.9 ± 3.4
Winter	0.7 ± 32.8	5.0 ± 116.8	-2.2 ± 2.9	0.7 ± 32.8	6.7 ± 116.7	-3.9 ± 4.3

Table2. (Supp). A_T and C_T mean values in the BoM (SOLEMIO) without LSE values. Salinity-normalised changes in nA_T and nC_T were calculated by dividing by in situ salinity and multiplying by 38. SD stands for standard deviation.

	Depth	AT Ø LSE [µmol.kg ⁻¹]	CT Ø LSE [µmol.kg ⁻¹]	nAT Ø LSE [µmol.kg ⁻¹]	nCT Ø LSE [µmol.kg ⁻¹]
SOLEMIO (2016 – 2018)	Surface	2584 ± 19	2289 ± 17	2570 ± 17	2277 ± 27
	Bottom	2582 ± 17	2302 ± 20	2567 ± 17	2288 ± 20

- First study of the variability of the carbonate system in the Bay of Marseille.
- The Bay of Marseille acts as a sink of atmospheric CO₂ at the annual scale.
- Temperature is the main contributor to the air-sea CO₂ exchange variability.

Journal Pre-proof

Declaration of interests

The authors declare that they have no known competing financial interests or personal relationships that could have appeared to influence the work reported in this paper.

The authors declare the following financial interests/personal relationships which may be considered as potential competing interests:

Journal Pre-proof